PREPARATION AND MORPHOLOGICAL STUDY OF COMPOSITE NANO-PARTICLES MADE OF HOMOPOLYMERS

by

Nan Wang

A thesis submitted to the Department of Chemistry

In conformity with the requirements for

the degree of Master of Science

Queen's University

Kingston, Ontario, Canada

(August, 2008)

Abstract

Composite polymer particles were made of two or more polymers. If these polymers are incompatible, the particles after polymer phase segregation exhibit complex morphologies which determine their properties and applications. Such particles may have applications in both academia and industry.

In this work, polystyrene (PS)/ poly(2-cinnamoyloxyethyl methacrylate) (PCEMA) and poly(acetyloxyethyl methacrylate) (PAEMA)/PCEMA composite polymer particles are prepared by the evaporation of toluene from PS/PCEMA/toluene and PAEMA/PCEMA/toluene droplets dispersed in an aqueous solution containing surfactants. The surfactants used for the two systems are poly(glyceryl methacrylate)$_{100}$-*block*-poly(2-cinnamoyloxyethyl methacrylate)$_{15}$ (PGMA$_{100}$-*b*-PCEMA$_{15}$) and poly(glyceryl methacrylate)$_{300}$-*block*-poly(2-cinnamoyloxyethyl methacrylate-*ran*-acetyloxyethyl methacrylate)$_{37}$ (PGMA$_{300}$-*b*-P(CEMA-*ran*-AEMA)$_{37}$), respectively, for the PS/PCEMA and the PAEMA/PCEMA systems. The morphologies of the PS/PCEMA and PAEMA/PCEMA composite particles are analyzed by transmission electron microscopy (TEM), atomic force microscopy (AFM), and dynamic light scattering (DLS). The results indicate that the particles are polydisperse and of nanometer size. For the PAEMA/PCEMA particles, the preferred morphology is hemisphere, while for the PS/PCEMA system the morphology is a mixture of acorn and occluded core-shell. Based on Gibbs free energy theory, and knowing the corresponding surface tensions and interfacial tensions, the thermodynamic equilibrium morphologies for both kinds of

composite particles were found. Due to the uncertainty during measurements and calculations, and the influence of kinetic factors, the theoretical predictions agreed only partially with the experimental observations.

Acknowledgements

First, and most importantly, I am extremely grateful to my supervisor Prof. Guojun Liu who continuously helped me improve my skills and the quality of my work. His inspiration and his great efforts to explain things in a clear and simple way have greatly influenced my way of thinking and approach to this research. His advice on doing the experiments and constructive comments on each draft directly contributed to this study. He will be my mentor for a life time.

My special thanks also go to my committee member, Prof Simon A.M. Hesp and Prof. Ralph. A. Whitney for passing on their valuable ideas and knowledge to me.

Many thanks are extended to Caizhen Zou, my best friend, for introducing me to the Liu group.

I would like to thank Dr Jiwen Hu for guiding me into this project. Without his valuable training and assistance, I cannot imagine how many difficulties I would have met at the early stage. I wish to express my sincere gratitude to Dr Gabriel Njikang for always being there to answer my questions, and proofreading my writings at different stages. I am also grateful to Ms. Jian Wang, Yang Gao and Zhen Wang for their assistance with AFM analyses and theoretical calculations. I would also like to extend my thanks to my colleagues: Dr Ronghua Zheng, Dr Dehui Han, Dr Jiguang Zhang, Dr Yu Fu, Zhihan

Zhou, John Dupont, Heng Hu, Xiaoyu Li, Qiliang Peng, Qian Cui, Shubin Zhao for giving me their friendship and encouragement in the past two years.

I am grateful to Jun Qian, my best friend and teacher out of the Chernoff Building in Kingston. I have learned so much from her. I wish her all the best in the future from the bottom of my heart.

Last but not the least, I would like to give my heartfelt thanks to my parents in China. Thank you, Dad and Mom, for your unconditional love. You have done your best to better educate me, and have always encouraged me to pursue my goals and assured me that you are just a phone call away. Your caring, giving, patience, and understanding helped me through every difficult and important moment. To you I owe a profound debt.

Table of Contents

List of Figures

List of Tables

Abbreviations

γ	surface tension
θ	contact angle
χ	Flory-Huggins interaction parameter
w/w	weight ratio
A	interfacial area
ABS	Acrylonitrile-Butadiene-Styrene
AFM	atomic force microscopy
CMC	critical micelle concentration
DLS	dynamic light scattering
ΔG	Gibbs free energy change
GPC	Gel Permeation Chromatography
HCl	hydrochloric acid
N	degree of polymerization
NMR	nuclear magnetic resonance
PAEMA	poly(acetyloxyethyl methacrylate)
PCEMA	poly(2-cinnamoyloxyethyl methacrylate)
PHEMA	poly(2-hydroxylethyl methacrylate)
PGMA-*b*-PCEMA	poly(glyceryl methacrylate)-*block*-poly(2-cinnamoyloxyethyl methacrylate)
PGMA-b-P(CEMA-ran-AEMA)	poly(glyceryl methacrylate)-*block*-poly(2-cinnamoyloxyethyl methacrylate-*ran*-acetyloxyethyl methacrylate)

PMMA	polymethyl methacrylate
PS	polystyrene
PSMA-b-PHEMA	poly(solketal methacrylate)-*block*-poly(2-hydroxylethyl methacrylate)
PtBA-*b*-PCEMA	poly(tert-butyl acrylate)-*block*-poly(2-cinnamoyloxyethyl methacrylate
SDS	sodium dodecyl sulfate
TEM	transmission electron microscopy
THF	tetradydrofuran
T_g	glass transition temperature
UV	ultraviolet light
Wa	work of adhesion

Chapter 1

Introduction

1.1 Research Objective and Organization of Thesis

Composite particles are particles made of two or more constituent materials with different physical or chemical properties. When the constituent materials include at least one polymer, they are called polymer composite particles. These kinds of particles have a wide range of applications. Their morphology is one of the key factors that control their physical properties, which in turn determine their applications. This thesis is focused on the preparation and morphological study of two kinds of composite polymer particles made from homopolymers of polystyrene (PS)/poly(2-cinnamoyloxyethyl methacrylate) (PCEMA) and poly(acetyloxyethyl methacrylate) (PAEMA)/PCEMA (Figure 1-1). The use of PCEMA in this work is mainly because of its photo-cross-linkable property. When irradiated by UV light, PCEMA domains crosslink. In this way, the structure can be locked. PCEMA has been used in much of the work presented by the Liu research group. The photo-cross-linkable property of PCEMA is an efficient technique to lock in nanostructures. Chapter one will introduce the general background of the subject. Chapter two will describe the preparation of the homopolymers, surfactants and composite polymer particles used in this study. The preparation of samples for contact angle measurement, TEM, AFM, and DLS are also included in chapter two. Chapter three will focus on the morphological and topographical study of PAEMA/PCEMA and

PS/PCEMA composite particles. Also, theoretical predictions, which are based on the Gibbs free energy change theory, will be given. Chapter four will draw conclusions and outline some future work.

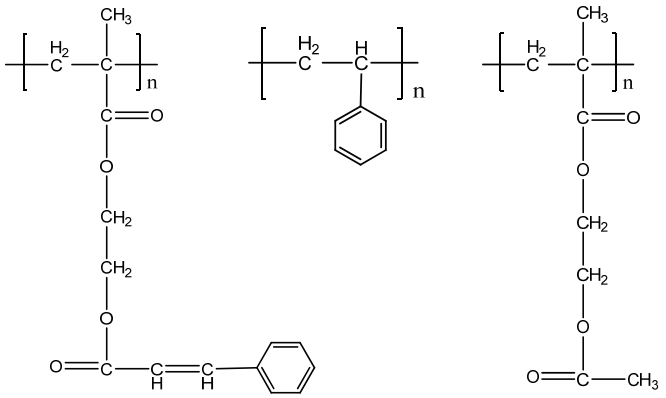

PCEMA PS PAEMA

Figure 1-1 Chemical structures of PCEMA, PS, and PAEMA

1.2 Composite Polymer Particles and Their Applications

1.2.1 Composite Polymer Particles Made from Incompatible Polymers

Composite polymer particles can be made from two or more incompatible polymeric phases, such as two homopolymers[1, 2] or the different blocks of a block copolymer[3]. When the incompatible phases segregate, the particles exhibit many complicated morphologies, including non-spherical morphologies. These kinds of composite particles have a wide range of applications in both academic and industrial areas. In the academic field, for example, non-spherical composite polymer particles made from homopolymers, which have unique responses to external fields due to their lack of spherical symmetry,

have been reported by many groups over the last twenty years. To date, reported morphologies include the snow-man, raspberry morphology, and so on[4-7]. Recently, composite particles made from block copolymers have been studied[3]. The self-assembly of block copolymers into polymer composite particles allows for the creation of unique nanostructures, as well as producing novel morphologies and properties. For example, Liu's group has reported spherical particles made from the diblock copolymer poly(tert-butyl acrylate)-*block*-poly(2-cinnamoyloxyethyl methacrylate) (PtBA-*b*-PCEMA), where the PtBA segregated into cylindrical domains dispersed in PCEMA[3] (Figure 1-2). After hydrolyzing the t-butyl group of the PtBA block, nano-channels were formed in the spheres. This complex internal structure could be used in conjunction with catalysts to increase the effective surface area. By exploiting the incompatibility of polymers, polymer nano- and microspheres with surface-segregated chains have also been made[8], which can be surface modified, potentially to express unique compounds such as amines or carboxylic acids which are desirable for use in diagnostic applications.

In the industrial area, one of the most common structures of these composite polymer particles is the "core-shell" morphology, which is widely used in impact modified plastics[9]. Particles with a soft crosslinked core surrounded by a hard copolymer shell have good properties. An example of an industrially used core-shell morphology composite polymer particle is one made from acrylonitrile-butadiene-styrene (ABS) resins.

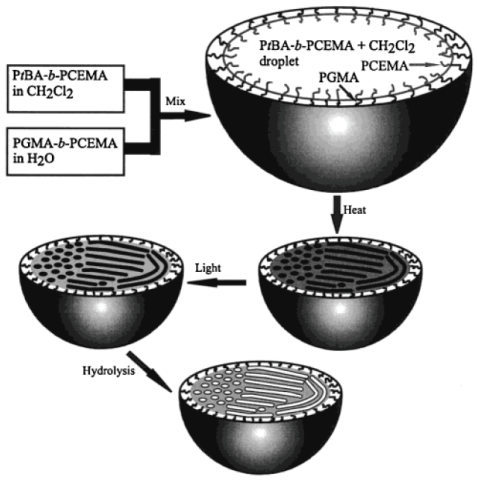

Figure 1-2 Composite polymer particle with nano-channel inside: preparation and processing of PtBA-*b*-PCEMA microspheres containing nanometer-sized cylindrical domains[3]

Two ways currently exist to produce composite particles from homopolymer blends. These are the synthetic route and the artificial route. In the synthetic route, polymer composite particles are prepared by the polymerization of a second monomer in the presence of the first polymer. Studies have shown that the morphology of particles can be either thermodynamically or kinetically controlled and is dependent on the experimental conditions[9]. Thermodynamic factors determine the equilibrium morphology of the final composite polymer particle while the kinetic factors determine the ease with which the preferred morphology is achieved.[10] Morphological transitions can be effected by varying the types of surfactants, initiators and polymers, or by varying the experimental parameters, such as reaction temperature.[11-16]

With the artificial route, polymers are first dissolved in an organic solvent, and then emulsified in water that contains surfactants and finally, the organic solvent is fully evaporated. During the process of solvent removal, the polymers phase separate and the minimization of the total interfacial free energy is the driving force for the system to reach the thermodynamic equilibrium morphology. By comparing the total interfacial free energy among thermodynamic equilibrium morphologies, it is possible to predict the preferred structures.[17-24] In order to take into account all potential morphologies, a more advanced method has been reported by Sundberg[25]. Unfortunately, until now only the PS/PMMA system has been fully studied. This may be due to the difficulties of interfacial tension measurement between polymers. For the PS/PMMA system, the experimental observations of the particles' morphologies are in good agreement with theoretical calculations.

1.2.2 Nano- and Micro- Capsules Formed of Liquid Core-Polymer Shell

Capsules formed with a liquid core and a polymer shell are one kind of polymer composite particles. These capsules can regulate the release of, or isolate the liquid core from, its surroundings. Such materials are very important in academic and industrial fields[26, 27]. An example of a liquid core-polymer shell capsule application is the protection offered to probiotic bacteria as they pass through high temperature food processing and passage through the digestive system. Nano- and micro-capsules have also been used as controlled release devices. The most common application is found in

the pharmaceutical industry where active drug species are released over an extended time scale using containers that have well-defined release properties.[28]

There are various methods to prepare capsules, such as the dendrimers approach[28], the template approach[29], the self-assembly approach, or the emulsion polymerization approach[30-33]. Reviews are available that discuss their advantages and disadvantages[28, 34]. By using these methods, different liquids can be encapsulated. In fact, limited by the preparation methods, the most common liquid core is an organic solvent. With the increasing interest in biological applications, more and more aqueous core polymer capsules have been reported[35, 36]. To prepare this kind of capsule, the preferred approach is the self-assembly method.

1.2.3 Polymer Metal Composite Particles

Another class of polymer composite particles is polymer metal composite particle; and with their unique properties, they have received more interest in recent years. With the development of nanoscience, research in this field has been greatly encouraged as nanoscale metal particles have shown special properties such as supermagnetism.

In order to make polymer metal composite particles, techniques such as chemical metal deposition[37], reduction of polymer metal ion complexes[38] and direct encapsulation[39] are employed. Limitations of the various preparation methods result in mainly two

morphologies for these kinds of composite particles, polymer core-metal shell and polymer shell-metal core particles.

1.3 Emulsion

An emulsion is a system that consists of two immiscible substances, in which one is dispersed in the other[40]. An emulsion is a subcategory of colloids and these terms are sometimes interchangeable. However, emulsions usually refer to systems where both the dispersed phase and continuous phase are liquids. For example, the most common emulsion is "oil-in-water". The process by which emulsions are prepared is called "emulsification".

Recently, due to many reasons, increasing efforts have been made to synthesize and apply polymer particles in a water phase. First, water is an inexpensive and inorganic solvent which is nontoxic and commonly found in the environment. Furthermore, many biomacromolecules exist only in an aqueous phase and thus, water dispersibility is the primary requirement to realize biology applications. These kinds of health, environmental and economical reasons, make polymer emulsions significant and necessary.

1.3.1 Stability of Emulsions

In order to prepare a stable emulsion, the droplets should resist two effects, one is molecular diffusion degradation or Ostwald ripening; the other is coalescence by

collisions.[41] The mechanisms of these two effects are different where the former one is a monomolecular process and the later one is a bimolecular mechanism.

Usually, after mechanical stirring, a heterogeneous fluid which contains surfactants forms an emulsion where the droplet sizes are not mono-disperse. The droplet size distribution is determined by Laplace pressure and increases with decreasing droplet size.[41] This polydispersity results in a net mass flux by diffusion, even when surfactants provide sufficient colloidal stability for the droplets.[41] The Laplace pressure in an oil-in-water emulsion is the difference between the pressure inside the monomer droplet, or polymer particle, and the pressure in the continuous medium due to the interfacial tension[42], where **r** is the particle radius and γ is interfacial tension.

$$P_{Laplace} = P_{inside} - P_{outside} = 2\gamma / r \qquad [1\text{-}1]$$

When diffusion degradation overcomes the droplets' stability, small particles dissolve into other nearby particles, which increase the average droplet size. For small droplets, this process is very fast[43]. Higuchi and Misra[44] have already theoretically studied the rate of growth of large particles and dissolution of small particles in emulsions and concluded that emulsion stability is determined by particle volume. When the particle volume increases, the stability increases proportionally. Size, polydispersity and solubility of the dispersed phase are significant factors that control the rate of Ostwald ripening.[41] Low polydispersity, small, hydrophobic oil droplets form stable emulsions in which there is a slow net exchange of mass between particles. Furthermore, Davis *et* al.[45] demonstrated

that by adding a third component that is an ultrahydrophobe, the stability of the emulsion increases. This phenomenon is explained by Raoult's law. Considering an emulsion system made from pure oil, smaller droplets have a higher vapor pressure than the larger ones. In order to reach the equilibrium state, the oil would pass from small particles to large ones. As the small particles become smaller, the Laplace pressure increases and correspondingly, the large particles become larger until the remaining smaller droplets reach a critical size which depends on the solubility of the oils. When a third component is added, which has a lower vapor pressure than the dispersed oil phase, the total vapor pressure is reduced, as defined by Raoult's law. As the small oil particles lose volume, the mole fraction of the ultrahydrophobe is increased in the small droplets and a related decrease in the large droplets, and thus the small droplets will have a reduced vapor pressure when compared to a droplet of pure oil of the same size.

Other effects that destabilize emulsions are coalescence and collision processes.[41] In colloid science, minimization of the collision effect is accomplished by adding appropriate surfactants which stabilize droplets by providing either electrostatic repulsion or steric hindrance.

1.3.2 Preparation of Emulsions

To prepare an emulsion, a fluid phase which contains surfactants and other components is premixed, and then mechanically mixed to deform and disrupt large droplets. During mixing, surfactants adsorb at the newly formed interfaces to stabilize the droplets.

There exist several techniques to prepare emulsions. The simplest is mechanical stirring such as with an omni-mixter or ultra-turrax, both of which are frequently used in the academic and industry fields[41]. However, these machines are not suitable for miniemulsion preparation, which consists of a stable emulsion having droplet diameters in the range of 50-500 nm[46]. In order to prepare a miniemulsion, much higher energies are required as the viscous resistance during agitation absorbs most of the energy and creates heat. A high force dispersion device, such as an ultrasonicator, is applied in order to obtain small and homogeneously distributed droplets. Even though these kinds of techniques are used to produce different sizes of emulsions, all of them are based on applying strong shearing stresses to the mixed fluid[47].

Membrane emulsification is a relatively novel technique for producing highly monodisperse particles. In a typical setup, the dispersed phase is forced to permeate into the continuous phase through a membrane having a uniform pore size distribution [48]. This technique was first investigated by Nakashima and Shimizu [49] in the late 1980s when they used a glass membrane and produced highly uniformly sized kerosene-in-water and

water-in-kerosene emulsions. This technique continues to be attractive because of its high effectiveness and low energy consumption.

1.3.3 Surfactants

Surfactants are usually amphiphilic compounds which contain hydrophobic tails and hydrophilic heads. Because of their amphiphilic properties, they dissolve in both organic solvents and water. In mixtures of immiscible solvents, surfactants exist at the liquid-liquid interface thereby reducing the interfacial tension between dissimilar phases. In the same way, by adsorbing at liquid-gas interface, they also reduce the surface tension of liquid. Consequently, surfactants are known as wetting agents.

Critical micelle concentration (CMC) is an important characteristic of amphiphilic surfactants as it refers to the concentration at which surfactants start to form micelles. When micelles form in water, their hydrophobic tails form a core that adsorb on oil droplets, while hydrophilic heads remain in contact with the water as an outer shell.

Amphiphilic surfactants can be grouped into four common categories according to the charge in their head groups when dissolved in water at neutral pH: anionic, cationic, non-ionic and amphoteric (Figure 1-4).[50] Surfactants having a negatively charge head are anionic, an example of which is sodium dodecyl sulfate (SDS) as well as other alkyl sulfate salts. When the head contains a positive charge, it is termed cationic, such as

cetrimonium bromide. Without a charge in the head group, the surfactant is called non-ionic, for example, fatty alcohols. If the head group contains both a positive and negative charge, such as cocamidopropyl betaine, it is termed amphoteric.

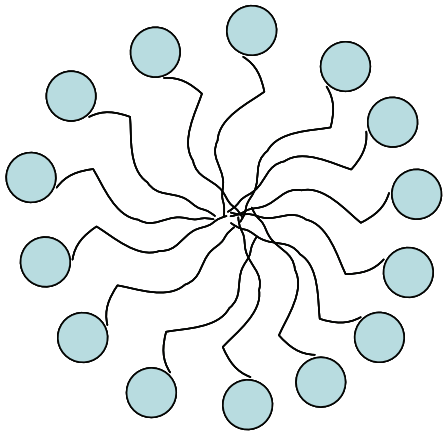

Figure 1-3 Surfactant molecules dissolve in water forming a micelle. The hydrophilic groups remain outside, shielding the hydrophobic groups

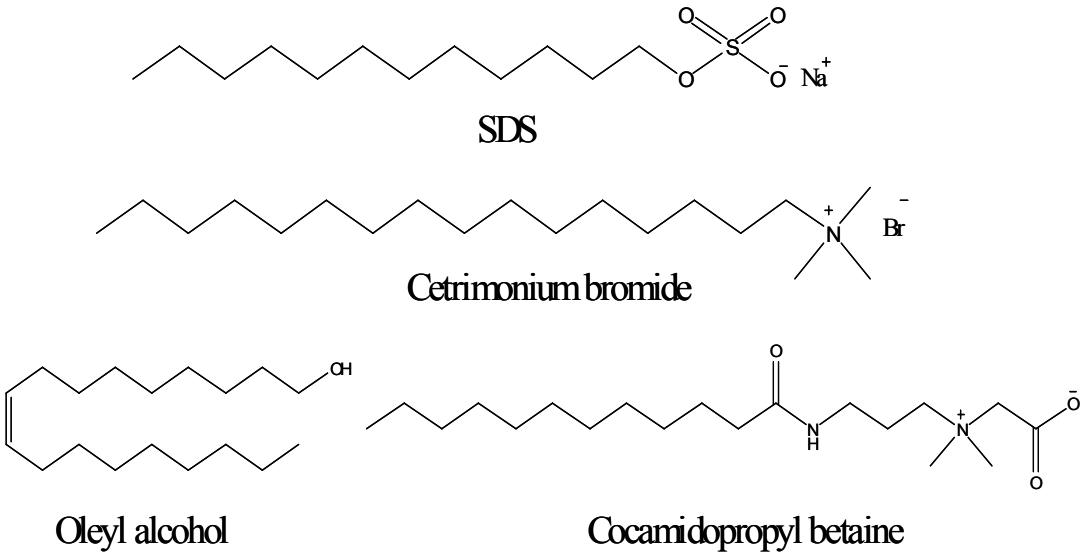

Figure 1-4 Chemical structures of four kinds of surfactants

Surfactants play an important role in academic, industrial and commercial applications, such as quantum dot coating, wetting, and detergents [51]. Commercially, the main uses of surfactant products are for the purpose of washing and cleaning. The next most common application for surfactants is in the field of cosmetics and pharmaceuticals. Surfactants are important in the production of creams and lotions because they function as emulsifiers. Another significant industry which uses surfactants is metal processing where surfactants are used as industry emulsifiers, surface-active agents, lubricants, cleaning agents and corrosion inhibitors.[52]

Recently, with the increasing attention given to environment problems, internationally, efforts are being made to make surfactants biodegradable and hence, more environmentally friendly.

1.4 Predicting Thermodynamic Equilibrium Morphology of Latex Polymer Particles Made from Two Homopolymers

1.4.1 Theory

To predict the thermodynamic equilibrium morphology of latex polymer particles made from two components, the Gibbs free energy change is the most commonly used method[9]. The Gibbs free energy change for morphological development during phase separation can be defined by combining the terms of enthalpic, entropic and surface free energies together. Due to the size difference between particles and molecules, the

influence of entropic changes can be neglected.[53] When analyzing the synthetic route, due to only considering the same stage of conversion of monomer to polymer, the enthalpic changes for differently shaped particles could be neglected. When the analysis is done for the artificial route during which no chemical reaction happens, the enthalpic changes could also be neglected. Also, usually consider the polymer 1 which is suspended in water and a bulk phase of polymer 2 to be the initial state. Since at the final state they are still phase separated, there is no mixing or demixing involved, the ΔS_{mix} and ΔH_{mix} could be neglected. This allows the Gibbs free energy change (ΔG) to be expressed only in terms of the total interfacial free energy change[54]. In Equation **1-2**, A_i is the area of the interface and γ_i is the interfacial tension at the *i*th interface. The $A_0\gamma_0$ term is the reference energy state.

$$\Delta G = \sum_i A_i\gamma_i - A_0\gamma_0 \qquad [1\text{-}2]$$

The most favorable morphology is the one that has the lowest predicted Gibbs free energy change when calculated with this equation. This method could be applied to the prediction for both the artificial and synthetic routes. Since at the final theoretical state, all of the organic solvent has been evaporated or the monomers have been converted completely, only the interfacial tensions between the two polymers and the water and the polymers against themselves need to be considered. Berg *et* al.[55], Sundberg and Muscato[1], and Winzor[23] have already laid the groundwork for this method's application to both the artificial and synthetic routes. Torza and Mason[56] attempted to use the spreading coefficients approach to predict droplet morphologies. They proposed that the

colloid particles were composed of two incompatible oils dispersed in water in which neither oil was soluble. By using spreading coefficients and the known interfacial tensions, they were able to predict the droplet morphologies. However, due to the inequalities involved in those coefficients this way is not so often used. Comparatively, the Gibbs free energy approach is more frequently employed because of its generality.

1.4.2 Methods to Determine Surface Tension and Interfacial Tension

In order to determine the interfacial tensions between polymer/water interfaces and the surface tension of polymers, methods such as contact angle measurement, the spinning drop method, the pendant drop method and the drop volume method are employed. Among them, the simplest is the contact angle measurement [57].

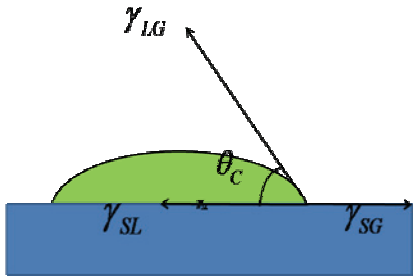

Figure 1-5 Contact angle

When a liquid droplet (L) contacts a surface substrate (S) surrounded by a gas/vapour (G), an angle, or the contact angle, is formed at the liquid/vapour/solid interface. (Figure 1-5) When thermodynamic equilibrium is reached, the chemical potential and the

interfacial energies of the three phases are equal. In the equilibrium state, Young's equation can be written as:

$$\gamma_{SG} = \gamma_{SL} + \gamma_{LG}\cos\theta \qquad [1\text{-}3]$$

Here γ_{SG}, γ_{SL} and γ_{LG} represent the solid-gas, solid-liquid and liquid-gas interfacial energies respectively, and in most literatures, γ_{LG} is written as γ_L. By knowing two of the interfacial energies and experimentally determining the contact angle, θ, one can determine the third, unknown interfacial energy.

An alternative method to solve interfacial tension can be achieved by combining Young's equation with geometric mean theory[60]. In this method, interfacial tension is defined in terms of the work of adhesion or *Wa* for an equilibrium system of a liquid with surface tension γ_L on a solid with surface tension γ_S. This adhesion work is equal to the geometric mean of the cohesive energy of the separated phases. Owens[58] and Kaelble[59] developed a geometric mean approximation method for testing surfaces with similar ionization potential and wrote the equation in the following format:

$$\begin{aligned} \gamma_{SL} &= \gamma_S + \gamma_L - 2\sqrt{\gamma_S^d \gamma_L^d} - 2\sqrt{\gamma_S^p \gamma_L^p} \\ \gamma_S &= \gamma_S^d + \gamma_S^p \\ \gamma_L &= \gamma_L^d + \gamma_L^p \end{aligned} \qquad [1\text{-}4]$$

Here, the surface tension consists of two parts, the dispersion (non-polar) energy component and the polar energy component. The former one is surface energy that results from non-polar interaction of molecules and the latter results from polar interaction. Combining this equation with Young's equation **1-3** yields

$$\gamma_L(1+\cos\theta) = 2\sqrt{\gamma_S^d \gamma_L^d} + 2\sqrt{\gamma_S^p \gamma_S^p} \qquad [1\text{-}5]$$

Thus, by measuring at least two different liquids having known dispersion and polar energies on the same solid surface, equation **1-5** can be solved and the surface tension of the polymer substrate can be calculated by determining its polar and non-polar energies simultaneously. It is more convenient to use equation **1-6** (Saito equation[60]) to calculate γ_s^d and γ_s^p for use in equation **1-4** and **1-5** where the parameters for liquids *i* and *j* are from literature.

$$\gamma_s^d = \frac{[(\frac{W_a}{2})_j(\sqrt{\gamma_L^p})_i - (\frac{W_a}{2})_i(\sqrt{\gamma_L^p})_j]^2}{D^2}$$
$$\gamma_s^p = \frac{[(\frac{W_a}{2})_j(\sqrt{\gamma_L^d})_i - (\frac{W_a}{2})_i(\sqrt{\gamma_L^d})_j]^2}{D^2} \qquad [1\text{-}6]$$
$$D = (\sqrt{\gamma_L^p})_i(\sqrt{\gamma_L^d})_j - (\sqrt{\gamma_L^d})_i(\sqrt{\gamma_L^p})_j$$
$$W_a = \gamma_L(1+\cos\theta)$$

In order to determine the interfacial tension between different polymers, Young's equation can be used by treating one of the polymers as a solid substrate and the other as a liquid. However, it is difficult to determine the contact angle between polymers. In order to solve this problem, Wu's equation [61] is used (Equation **1-7**), which is a harmonic mean approximation for both the dispersion and polar components and avoids the need for a contact angle. However, when compared to the interfacial tension between the polymer/water phases, the interfacial tension between polymers has a negligible effect on the prediction of the final morphology.

$$\gamma_{SL} = \gamma_S + \gamma_L - \frac{4\gamma_S^d \gamma_L^d}{\gamma_S^d + \gamma_L^d} - \frac{4\gamma_S^p \gamma_L^p}{\gamma_S^p + \gamma_L^p} \qquad [1\text{-}7]$$

1.5 Conclusions

In this chapter, the relevant information and background about composite polymer particles, their applications, preparation methods and theoretical predictions have been presented. In chapter two, the synthesis of homopolymers and surfactants used in this study, and the preparation of the composite polymer particles will be described. The interfacial tension measurements and preparation of specimen for TEM, AFM and DLS will also be included in the next chapter.

References

1. Sundberg, D. C.; Muscato, M. R.; *J. Appl. Polym. Sci.* **1990**, *41*, 1425
2. Okubo, M.; Yamaguchi, S.; Matsumoto, T.; *J. Appl. Polym. Sci.* **1986**, *31,* 1075
3. Lu, Z. H.; Liu, G. J.; Liu, F. T.; *Macromolecules* **2001**, *34*, 8814
4. Matsumoto, T.; Okubo, M.; Shibao, S.; *Kobunshi Ronbunshu* **1976**, *33,* 575
5. Okubo, M.; Izumi, J.; Takekoh, R.; *Colloid. Polym. Sci.* **1999**, *277*, 875
6. Cho, I.; Lee, K. W.; *J. Appl. Polym. Sci.* **1985**, *30*, 1903
7. Okubo, M; Ando, M.; Yamada, A.; Katsuta, Y.; Matsumoto, T.; *J. Polym. Sci. Polym. Lett. Ed.* **1981**, *19*, 143
8. Zheng, R.H.; Liu G. J.; *J. Am. Chem. Soc.* **2005,** *127*, 15358
9. Sundberg, D.C.; Durant, Y.G.; *Polym.React. Eng.* **2003**, *11*, 379
10. Chen, Y.-C.; Dimonie, V. L.; El Aasser, M. S ;*Pure & Appl. Chem.* **1992**, *64,*1691
11. Min, T. I.; Klein, A.; El Aasser, M. S.; Vanderhoff, J. W.; *J. Polym. Sci. Polym. Lett. Ed.* **1983**, *21*, 2845
12. Dimonie, V.; El Aasser, M. S.; Klein, A.; Vanderhoff, J. W.; *J. Polym. Sci. Polym. Chem. Ed.* **1984**, *22*, 2197
13. Muroi, S.; Hashimoto, H.; Hosoi, K.; *J. Polym. Sci. Polym. Chem. Ed.* **1984**, *22*, 1365
14. Merkel, M. P.; Dimonie, V. L.; El Aaasser, M. S.; Vanderhoff, J. W.; *J. Polym. Sci., Part A: Polym. Chem.* **1987**, *25*, 1755
15. Okubo, M.; Ikegami, K.; Yamamoto, Y.; *Colloid Polym. Sci.* **1989**, *267*, 193
16. Lee, S.; Rudin, A.; *Makromol. Chem., Rapid. Commun.* **1989**, *10*, 655
17. Chen, Y.-C.; Dimonie, V. L.; El Aasser, M. S.; *Macromolecules* **1991**, *24*, 3779
18. Chen, Y.-C.; Dimonie, V. L.; El Aaasser, M. S.; *J. Appl. Polym. Sci.* **1991**, *42*, 1049
19. Jonsson, J.-E. L.; Hassander, H.; Jansson, L. H.; Tornell, B.; *Macromolecules* **1991**, *24*, 126
20. Chen, Y.-C.; Dimonie, V. L.; El Aasser, M. S.; *J. Appl. Polym. Sci.* **1992**, *45*, 487
21. Chen, Y.-C.; Dimonie, V. L.; El Aasser, M. S.; *J. Appl. Polym. Sci.* **1992**, *46*, 691
22. Winzor, C. L.; Sundberg, D. C.; *Polymer* **1992**, *33*, 3797
23. Winzor, C. L.; Sundberg, D. C.; *Polymer* **1992**, *33*, 4269
24. Durant, Y. G.; Guillot, J.; *Colloid Polym. Sci.* **1993**, *271*, 607
25. Durant, Y. G.; Sundberg, D. C.; *J. Appl. Polym. Sci.* **1995**, *58*, 1607
26. Caruso, F.; Trau, D.; Mohwald, H.; Renneberg, R.; *Lagumuir* **2000**, *16*, 1485
27. www.laboratorytalk.com, "laboratorytalk", Frost and Sullivan, August 14th 2002
28. Meier, M.; *Chem. Soc. Rev.* **2000**, *29*, 295
29. Huang, H. Y.; Remsen, E. E.; Kowalewski, T.; Wooley, K. L.; *J. Am. Chem. Soc.* **1999**, *121*, 3805
30. Okubo, M.; Minami, H.; *Colloid Polym. Sci.*, **1998**, *276*, 638
31. Kong, X. Z.; Kan, C. Y.; Li, H. H.; Yu, D. Q.; Juan, Q.; *Polym. Adv. Technol.*, **1997**, *8*, 627
32. Doashi, T.; Yeh, F.; Ying, Q.; Ichikawa, K.; Chu, B.; *Langmuir*, **1995**, *11*, 4278
33. Emmerich, O.; Hugenerg, N.; Schmidt, M.; Sheiiko, S. S.; Baumann, F.; Deubzer, B.;

Weis, J.; Ebenhoch, J.; *Adv . Mater.*, **1999,** *11*, 1299
34. Yow, H. N.; Routh, A. F.; *Soft Matter,* **2006**, *2*, 940
35. Hotz, J.; Meier, W.; *Adv. Mater.*, **1998**, *10*, 1387
36. Hetzer, M.; Clausen-Schaumann, H.; Bayerl, S.; Bayerl, T. M.; Camps, X.; Vostrowsky, O.; Hisch, A.; *Angew. Chem., Int. Ed.*, **1999**, *38*, 1962
37. Warshawsky, A.; Upson, D. A.; *J. Polym. Sci. Polym. Chem.* **1989**, *27*, 2963
38. Tamai, T.; Sakurai, S.; Hirota, Y.; Nishiyama, F.; Yasuda, H.; *J. Appl. Polym. Sci.* **1995,** *56,* 441
39. Gupta, P. K.; Hung, C. T.; Lam, F. C.; Perrier, D. G. *Int. J. Pharm.* **1988**, *43*, 167
40. Bibette, J.; Leal-Calderon, F.; Schmitt, V.; Poulin, P.; In *Emulsion Science*; Hohler, G.; Fukuyama, H. Eds; New York, Springer, **2007**
41. Antonietti, M.; Landfester, K.; *Prog. Polym. Sci.* **2002**, *27*, 689
42. Kralchevsky, P. A.; Danov, K. D.; Denkov, N. D.; In *Surface and Colloid Chemistry;* Bridi, K. S. Ed; CRC Press, Boca Raton, **1997**, p.341
43. Mishchuk, N. A.; Verich, S. V.; Dukhin, S. S.; *J. Dispersion Sci. Technol*, **1997**, *18*,517
44. Higuchi, W. I.; Misra, J.; *J. Pharm. Sci.* **1962**, *51*, 459
45. Davis, S. S.; Round, H. P.; Purewal, T. S.; *J. Colloid. Interface Sci.* **1981**, *80*, 508
46. Landfester, K.; Bechthold, N.; Tiarks, F.; Antonietti, M.; *Macromolecules* **1999**, *32*, 5222
47. Leal-Calderon, F.; Thivilliers, F.; Schmitt, V.; *Curr. Opin. Colloid Interface Sci.,* **2007**, *12*, 206
48. Charcosset, C.; Fessy, H.; *Rev. Chem. Eng.* **2005**, *21*, 1
49. Nakashima, T.; Shimizu, M.; *Ceram. Jpn.* **1986,** *21*, 408 (in Japanese)
50. Schmalstieg, A.; Wasow, G. W.; Steichen, D. S.; Cox, M. F.; Floyd, D. T.; Schunicht, C,; Gruening, B.; In *Handbook of Applied Surface and Colloid Chemistry*; Holmberg, K.; Shah, D.O.; Schwuger, M. J. Eds; New York, Wiley, **2002**
51. *US Patent* 5 540 865, to The Procter & Gamble Company, **1996**
52. Huber, L.; In *Handbook of Applied Surface and Colloid Chemistry*; Holmberg, K.; Shah, D.O.; Schwuger, M. J. Eds; New York, Wiley, **2002**
53. Saito, N.; Kagari, Y.; Okubo, M. *Langmuir*, **2007**, *23*, 5914
54. Berg, J.; Sundberg, D. C.; Kronerg, B. J.; *Microencap.* **1989,** *6666*, 327
55. Berg, J.; Sundberg, D. C.; Kronberg, B. J.; *Polym. Mater. Sci. Eng.* **54**, 367
56. Torza, S.; Mason, S. G.; *J. Colloid Interface Sci.* **1970**, *33*, 67
57. Kwok, D. Y.; Neumann, A. W.; *Ad. Colloid Interface Sci.* **1999,** *81***,** 167
58. Owens, D. K.; *J. Appl. Polym. Sci*. **1970**, *14*, 1725
59. Kaelle, D. H., *Physical Chemistry of Adhesion*, Wiley-Interscience, **1971**
60. Saito, M.; *Text. Res. J.* **1983,** *53***,** 54
61. Wu, S.; *J. Colloid Interface Sci*. **1969,** *31***,** 153

Chapter 2
Experimental Details

2.1 Introduction

In this work, the artificial route was used to prepare polymer composite particles from homopolymers. Two pairs of homopolymers, polystyrene (PS)/ poly(2-cinnamoyloxyethyl methacrylate) (PCEMA) and poly(acetyloxyethyl methacrylate) (PAEMA)/PCEMA, were used to prepare composite particles. The surfactants used for the two systems were poly(glyceryl methacrylate)$_{100}$-*block*-poly(2-cinnamoyloxyethyl methacrylate)$_{15}$ (PGMA$_{100}$-*b*-PCEMA$_{15}$) and poly(glyceryl methacrylate)$_{300}$-*block*-poly(2-cinnamoyloxyethyl methacrylate-*ran*-acetyloxyethyl methacrylate)$_{37}$ (PGMA$_{300}$-*b*-P(CEMA-*ran*-AEMA)$_{37}$), respectively.

This chapter focuses on the synthesis of polymers used in the work and the interfacial tension measurements of these homopolymers against water, ethylene glycol and polyethylene glycol. The preparation of specimen for TEM, AFM, and DLS are also included as techniques in this chapter.

2.2 Materials and Methods

2.2.1 Reagent

A.C.S. reagent grade pyridine was purchased from Fisher Scientific and dried by passing through two columns of alumina in a Grubb's type system for solvent purification. A.C.S.

reagent grade toluene and cinnamoyl chloride 98% were purchased from Sigma-Aldrich, acetic anhydride puriss 99.0% was purchased from Fluka, and A.C.S. reagent grade methanol was purchased from Fisher Scientific, and all of the above were used as supplied. A.C.S. reagent grade poly(2-hydroxyethyl methacrylate) (PHEMA, Mw=300000) and polystyrene (PS, Mw=200000) were purchased from Sigma-Aldrich and Pressure Chemical, respectively. PHEMA was dried overnight before using.

2.2.2 Polymer Synthesis and Characterization

PS, PHEMA and poly(solketal methacrylate)-*block*-poly(2-hydroxylethyl methacrylate) (PSMA-*b*-PHEMA) were used for these studies. The procedures used to purify the monomers and prepare diblock copolymer PSMA-*b*-PHEMA have been reported before and are thus not repeated here in detail[1]. PCEMA, PAEMA and the corresponding diblock copolymer surfactants were prepared by functionalizing these polymers as described later, and the results were checked by gel permeation chromatography (GPC) and nuclear magnetic resonance (NMR).

2.2.2.1 Preparation of Homopolymers

To prepare PCEMA, PHEMA 200 mg was mixed with 385 mg cinnamoyl chloride and dissolved in 2 mL of dry pyridine. The mixture was stirred overnight before it was centrifuged to remove the pyridinium salt. Then the polymer solution was added to

excess methanol to precipitate out PCEMA. The polymer was then dried at room temperature under vacuum.

To prepare PAEMA, PHEMA 200 mg was dissolved in 2 mL of dry pyridine. Under magnetic stirring, 0.25 mL acetic anhydride was added dropwise. After 3 hours, the polymer solution was added to excess methanol to precipitate out PAEMA. The polymer was then dried at room temperature under vacuum.

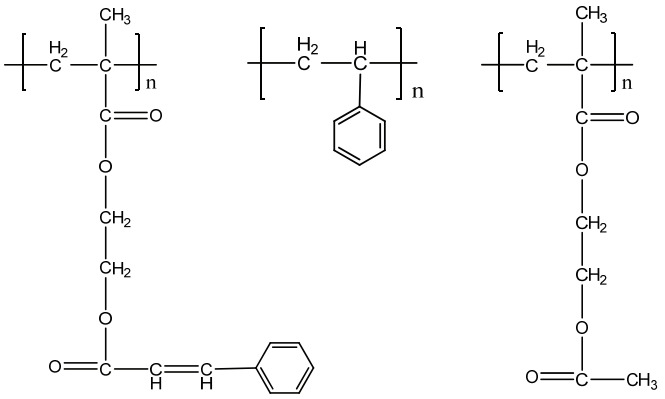

PCEMA PS PAEMA

Figure 2-1 Chemical structures of PCEMA, PS and PAEMA

2.2.2.2 Preparation of $PGMA_{300}$-*b*-P(CEMA-*ran*-AEMA)$_{37}$

To prepare $PGMA_{300}$-*b*-P(CEMA-*ran*-AEMA)$_{37}$, $PSMA_{300}$-*b*-$PHEMA_{37}$ was used. Half of the PHEMA block of the copolymer was converted to PCEMA using a similar procedure to that described above. $PSMA_{300}$-*b*-$PHEMA_{37,}$ 400 mg was mixed with 30 mg cinnamoyl chloride and dissolved in 3 mL of dry pyridine. The mixture was stirred over

night. Then the polymer solution was dropped onto ice crystals to precipitate the polymer. The polymer precipitate was rinsed with methanol before vacuum drying. The rest of the PHEMA was converted to PAEMA by reacting with acetic anhydride. In a typical procedure, 300 mg $PSMA_{300}$-*b*-P(CEMA-*ran*-HEMA)$_{37}$ was dissolved in 2 mL of dry pyridine. Under magnetic stirring, 0.1 mL acetic anhydride was added. After 3 hours, the polymer solution was added to excess methanol to precipitate out polymer. To hydrolyze the PSMA groups, 120 mg polymer was dissolved in 6 mL THF. To this solution was added 1.5 mL of a 6 M aqueous HCl solution. The mixture was stirred at room temperature for 3 hours, and then dialyzed against methanol (Spectra/Pro, molar mass cutoff 14000 g/mol) to remove water, HCl, and THF. After 1 day, the mixture was concentrated under reduced pressure and then added to ethyl ether to precipitate out $PGMA_{300}$-*b*-P(CEMA-*ran*-AEMA)$_{37}$. The polymer was dried at room temperature under vacuum. ^{1}H NMR was used to determine reaction progress.

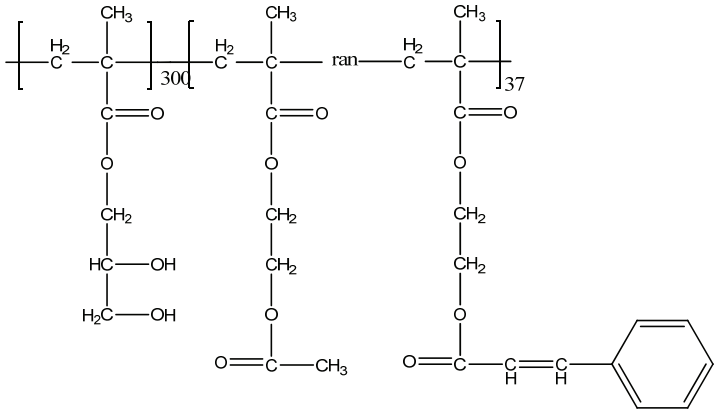

Figure 2-2 Chemical structure of $PGMA_{300}$-*b*-P(CEMA-*ran*-AEMA)$_{37}$

2.2.2.3 Preparation of $PGMA_{100}$-*b*-$PCEMA_{15}$

To prepare $PGMA_{100}$-$PCEMA_{15}$, $PSMA_{100}$-*b*-$PHEMA_{15}$ 200 mg was mixed with 35 mg cinnamoyl chloride and dissolved in 2 mL of dry pyridine. The mixture was stirred overnight before it was centrifuged to remove the pyridinium salt. Then the polymer solution was added to excess methanol to precipitate out polymer. The polymer was then dried at room temperature under vacuum. To hydrolyze the PSMA groups, 120 mg polymer was dissolved in 6 mL THF. To it was added 1.5 mL of a 6 M aqueous HCl solution. The mixture was stirred at room temperature for 3 hours, and then dialyzed against methanol (Spectra/Pro, molar mass cutoff 14000 g/mol) to remove water, HCl, and THF. After 1 day, the mixture was concentrated under reduced pressure and then added to ethyl ether to precipitate out $PGMA_{100}$-*b*-$PCEMA_{15}$. The polymer was dried at room temperature under vacuum

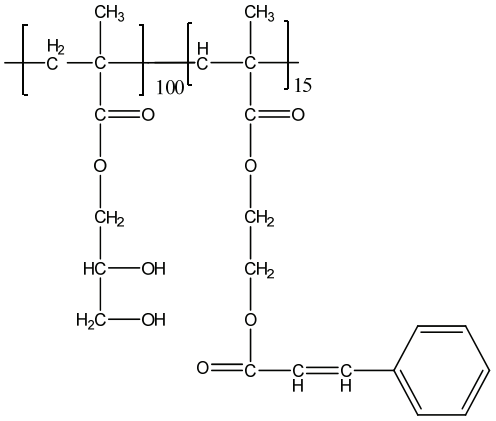

Figure 2-3 Chemical structure of $PGMA_{100}$-$PCEMA_{15}$

2.2.3 Preparation of PAEMA/PCEMA Composite Particles

All preparations were carried out in a 100 mL, three-neck round-bottom flask immersed in an oil bath. A hemispherically shaped Teflon stirrer was mounted to one end of a

mechanical stirring shaft and inserted into the flask via the middle joint of the flask[2]. Water (10 mL) containing 5 mg of surfactant was added into the flask. While stirring at 1000 rpm 0.40 mL of toluene containing 5 mg of each of the homoplymers was added dropwise. After stirring at room temperature for 30 min, the system was heated to 80 °C and mechanically stirred at 1000 rpm for 1 h, after which, the temperature was raised to 90 °C to evaporate toluene. To make composite particles with different homopolymer weight ratio, the same procedure was used.

2.2.4 Preparation of PS/PCEMA Composite Particles

The method used to prepare PS/PCEMA composite particles was similar to the above mentioned procedures for the preparation of PAEMA/PCEMA particles. First, 5 mg of each of the homopolymers were dissolved together in 0.4 mL of toluene to make a 25 mg/mL organic phase. This was then mixed with 10 mL water containing 4 mg surfactants under mechanical stirring to yield a cloudy mixture. The mixture was sonicated for 10 minutes to yield an emulsion. This emulsion was then heated to 80 ºC and mechanically stirred at 1000 rpm for 1 hour, after which, the temperature was raised to 90 $^{\circ}$C to evaporate toluene. This same procedure was used to prepare composite particles with different homopolymer weight ratio.

2.2.5 Measurements and Techniques

Size exclusion chromatographic analysis was carried out at 22 ^{o}C on a Waters 515 system equipped with two columns (Waters Styragel HT 4 and μStyragel 500 Å) and a differential refractometer (Water 2410). The eluant used was THF and the calibration standards used were monodisperse PS samples. Proton nuclear magnetic resonance (^{1}H NMR) spectra were obtained on a Bruker Avance 400 MHz spectrometer with either deuterated chloroform or pyridine as the solvent. A Brookhaven BI-200 SM instrument equipped with a BI-9000AT digital correlator and a He-Ne laser (632.8 nm) was used to do dynamic light scattering measurements at 22 °C. The measurements were done at an angle of 90°. The samples were purified by filtration through 0.45 μm pore-size Titan2 cellulose filters. The hydrodynamic diameter D_h and polydispersity K_2^2/K_4 were estimated by using a cumulant method[3] to analyze the data. Tapping mode AFM was performed with a Veeco multimode microscope equipped with a Nanoscope IIIa controller. A silicon tip was employed with a force constant and oscillating frequency of approximately 40 N/m and 300 kHz, respectively.[4] Specimens for AFM were prepared by aspirating sample solutions onto freshly washed silicon wafer. The silicon wafer was washed by H_2SO_4/H_2O_2 solution. In a typical recipe, the silicon wafer was immersed in H_2SO_4/H_2O_2 (v: v, 7:3) solution and heated at 70 ^{o}C for 1 hour. Then the silicon wafer was washed by distilled water to remove the acid. TEM measurements were carried out on a Hitachi H-7000 instrument operated at 75 kV. The specimens for TEM were prepared by aspirating the sample solutions on nitro cellulose coated copper grids. The TEM specimens were stained with OsO_4 vapor for 1 h before observations.

VCA-Optima Surface Analysis Systems were used for static contact angle measurements. All experiments were carried out at 22 °C. Water, ethylene glycol and polyethylene glycol were used as the probe liquids and their contact angles were measured at five different positions for each polymer substrate and averaged. The droplet volume was selected to be 1.5 μL so that gravity effect is negligible. The polymer substrates of PS, PCEMA and PAEMA were made by spin-coating method. In a typical process, the homopolymers were dissolved in chloroform to make 200 mg/mL concentrated solution. After spin-coating, the polymer films were prepared. The flat substrates were formed after these polymer films being annealed at 125°C under vacuum for 3 days.

References

1. Liu, F. T.; Liu, G. J.; *Macromolecules,* **2001,** *34,* 1302
2. Liu, G. J.; Yang, H. S.; Zhou, J. Y. *Biomacromolecules*, **2005**, *6,* 1280
3. Berne, B. J.; Pecora, R. *Dynamic Light Scattering with Applications to Chemistry, Biology, and Physics*; Dover Publications, Inc.: Mineola, NY, 1976
4. Njikang, G.: Liu, G. J.; Gao, J. *Macromolecules*, **2007**, *40*, 9174

Chapter 3
Results and Discussions

3.1 Introduction

This chapter focuses on the morphology, topography studies and calculations of free energy change of PS/PCEMA and PAEMA/PCEMA composite polymer particles. To study the influence of the component weight ratio on the final morphology, three batches of composite polymer particles, consisting of 75%, 50%, and 25% PCEMA homopolymers by weight were made for both polymer mixtures. To visualize the morphology of the particles, transmission electron microscopy (TEM) was employed. With the help of aimed staining, the position of each domain is clearly shown. In order to analyze the topography, atomic force microscopy (AFM) was employed. To analyze the polydispersity and determine the hydrodynamic diameter when particles were formed in aqueous solution, dynamic light scattering (DLS) was used. Thus, from these three methods, comprehensive morphological and topographical analyses of the two composite particle systems were obtained, after which, the calculations of free energy change will be presented.

3.2 Polymer Characterization

Homopolymer PCEMA, PAEMA and PS were used in this study. PS standards were obtained from Chemical Press and used without further purification. PCEMA was made

by reacting PHEMA with 1.5 molar equivalents of cinnamoyl chloride in dry pyridine at room temperature overnight. Then the solution was centrifuged to remove pyridinium salt before it was added to excess methanol to precipitate out PCEMA. PAEMA was prepared by reacting PHEMA with 1.5 molar equivalents of acetic anhydride in dry pyridine at room temperature for 3 hours. The polymer solution was added to excess methanol to precipitate out PAEMA. Both PCEMA and PAEMA were then dried at room temperature under vacuum. Block copolymer $PGMA_{300}$-*b*-$P(CEMA\text{-}ran\text{-}AEMA)_{37}$ and $PGMA_{100}$-*b*-$PCEMA_{15}$ were used as surfactants in this study. To synthesize these two kinds of polymers, $PSMA_{300}$-*b*-$PHEMA_{37}$ and $PSMA_{100}$-*b*-$PHEMA_{15}$ were used as precursors, respectively. PHEMA block of the copolymer was first converted to PCEMA using a similar procedure to that described above. To obtain the random copolymer, the rest of the PHEMA was converted to PAEMA by reacting with acetic anhydride. Then PSMA block of the copolymers were hydrolyzed in THF containing aqueous hydrochloric acid solution to PGMA, after which the mixtures were dialyzed against methanol. After one day, the solutions were concentrated and then added to ethyl ether to precipitate out block copolymers.

Homopolymers and block co-polymers were characterized by gel permeation chromatography (GPC) and ^{1}H nuclear magnetic resonance (NMR) with the results summarized in Table 3-1. In the GPC analysis, block co-polymers were measured in THF in the PSMA-*b*-PCEMA form. Since both PAEMA and PCEMA were synthesized from

the same PHEMA, and in the GPC analysis PHEMA was measured in the PCEMA form, in Table 3-1 only PCEMA result was shown. For the NMR analysis, the block co-polymers were measured in the PGMA-*b*-P(AEMA-ran-CEMA) and PGMA-*b*-PCEMA form.

Table 3-1 Characterization of Polymers

Sample	M_n by GPC (g/mol)	M_w by GPC (g/mol)	M_w/M_n by GPC	m/n by NMR
$PSMA_m$-*b*-$PCEMA_n$[a]	6.3×10^4	7.0×10^4	1.10	8.1/1
$PSMA_m$-*b*-$PCEMA_n$[b]	2.2×10^4	2.3×10^4	1.06	6.7/1
PCEMA	5.5×10^4	1.1×10^5	2.08	

[a] For ^{1}H NMR the PGMA-*b*-P(AEMA-*ran*-CEMA) form was used. It was also used as the surfactant for PCEMA/PAEMA composite particles.
[b] For ^{1}H NMR the PGMA-*b*-PCEMA form was used. It was also used as the surfactant for PCEMA/PS composite particles.

3.3 Transmission Electron Microscopy

In this section, TEM images of the two kinds of composite polymer particles will be given. Since electrons can be transmitted through both polymers, the inner structures are imaged by TEM. In order to distinguish the location of each homopolymer, OsO_4 was used for selective staining. As a strong oxidant, OsO_4 preferentially reacts with unsaturated carbon-carbon bonds, such as those found in PCEMA and, in this way, "stains" them. Since osmium atoms are extremely electron dense, their presence scatters electrons out of the optical path, which results in TEM images where the darker areas are PCEMA and lighter parts being PS or PAEMA domains.

TEM samples were prepared by aspirating a fine mist of a dilute solution of composite particles onto nitro-cellulose film-coated copper grids and stained by OsO_4 vapor for 1 hour. Figures 3-1, 3-2 and 3-3 show TEM images of OsO_4 stained PAEMA/PCEMA composite particles obtained after toluene evaporation. The weight ratios between PAEMA and PCEMA for these three samples are 1:3, 1:1 and 3:1, respectively.

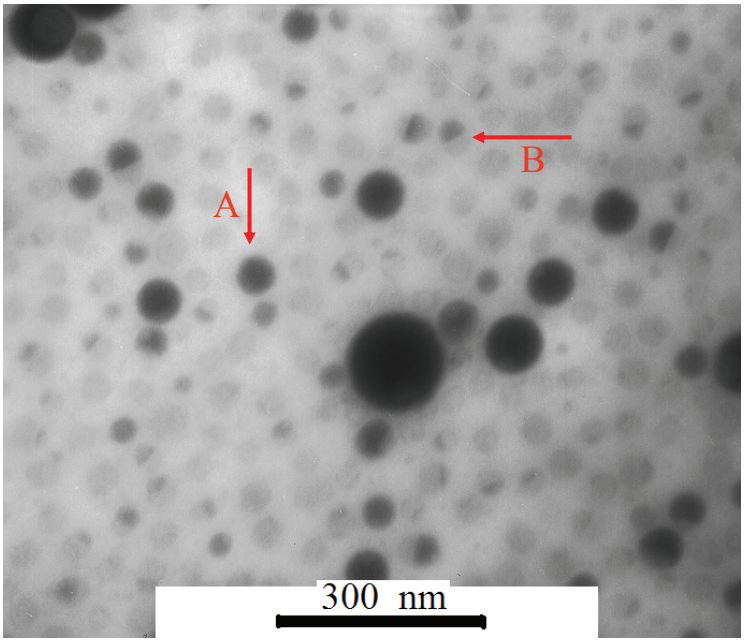

Figure 3-1 TEM micrograph of OsO_4 stained PAEMA/PCEMA (1:3, w/w) polymer composite particles

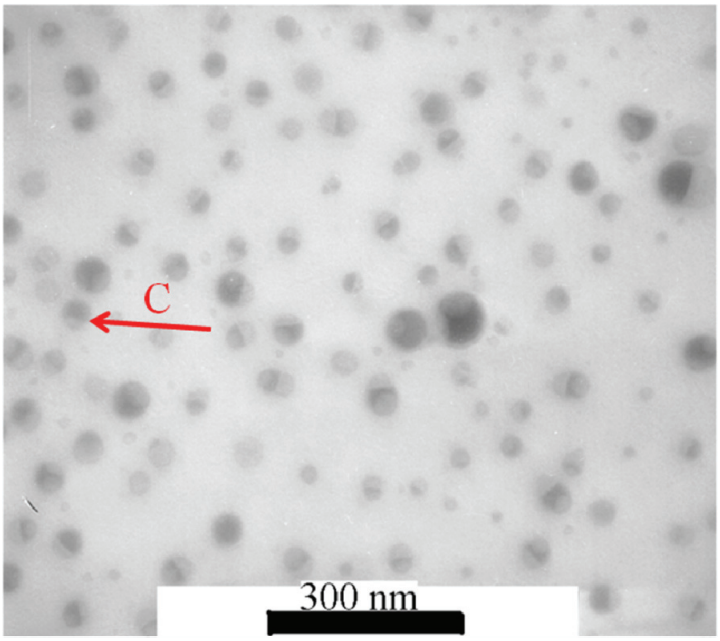

Figure 3-2 TEM micrograph of OsO_4 stained PAEMA/PCEMA (1:1, w/w) polymer composite particles

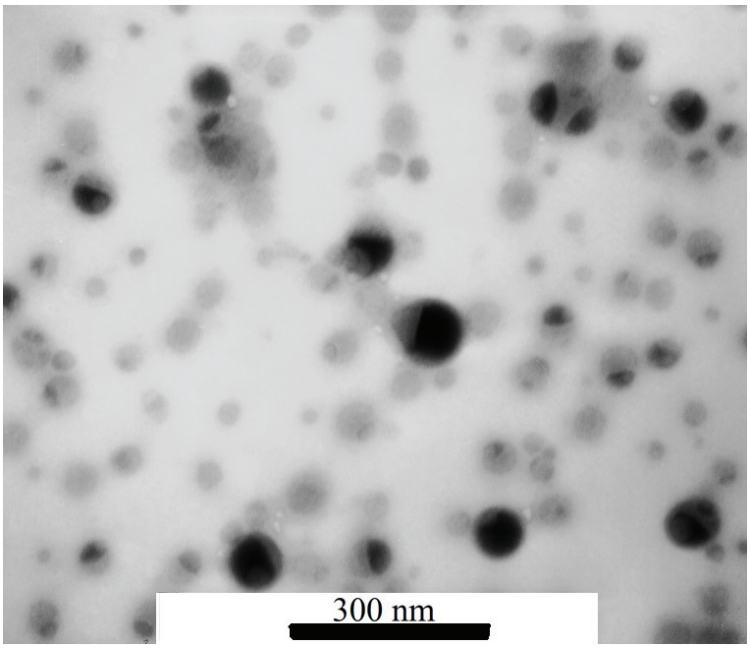

Figure 3-3 TEM micrograph of OsO_4 stained PAEMA/PCEMA (3:1, w/w) polymer composite particles

Figures 3-1, 3-2, and 3-3 illustrate that the preferred morphology for PAEMA/PCEMA composite particles after toluene evaporation is hemispherical for the weight ratios studied. For example, in Figure 3-1 arrow **B** shows this kind of morphology. For particles containing 75%, 50%, and 25% PCEMA homopolymers (weight ratio), the average diameters ± standard deviation were 46 ± 12 nm, 46 ± 12 nm, and 49 ± 18 nm respectively. This technique gives the diameter d_{TEM} of the PAEMA/PCEMA core only since the PGMA corona is invisible in TEM images.

Figures 3-4, 3-5 and 3-6 show TEM images of OsO_4 stained PS/PCEMA composite particles obtained after toluene evaporation. The weight ratios between PS and PCEMA were 1:3, 1:1 and 3:1 for Figure 3-4, 3-5 and 3-6 respectively.

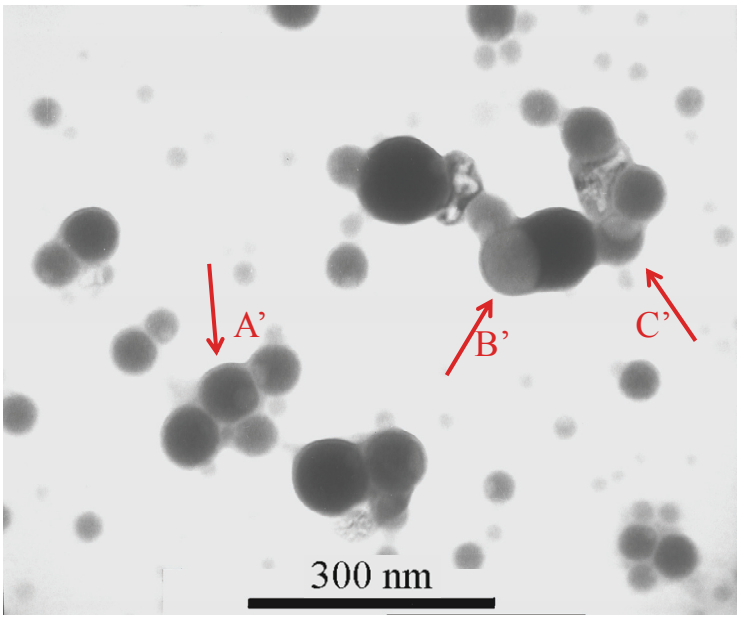

Figure 3-4 TEM micrograph of OsO_4 stained PS/PCEMA (1:3, w/w) polymer composite particles

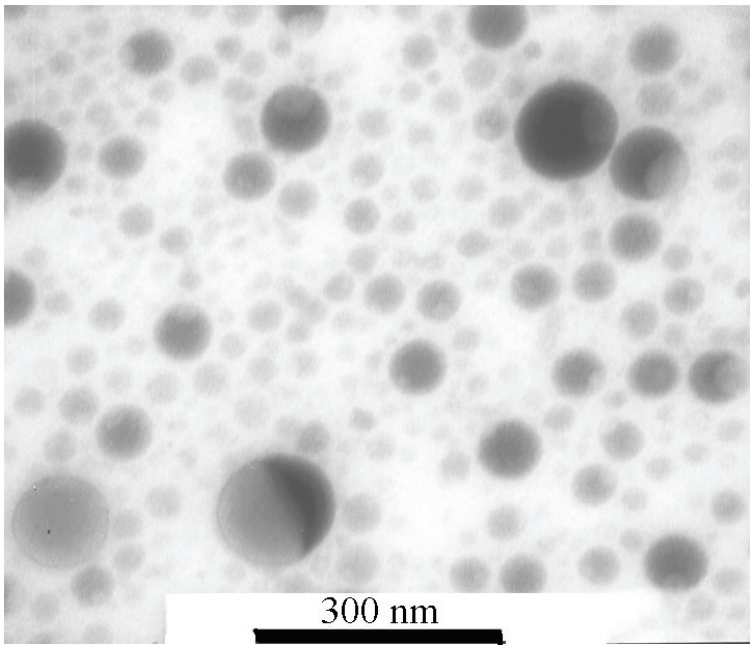

Figure 3-5 TEM micrograph of OsO_4 stained PS/PCEMA (1:1, w/w) polymer composite particles.

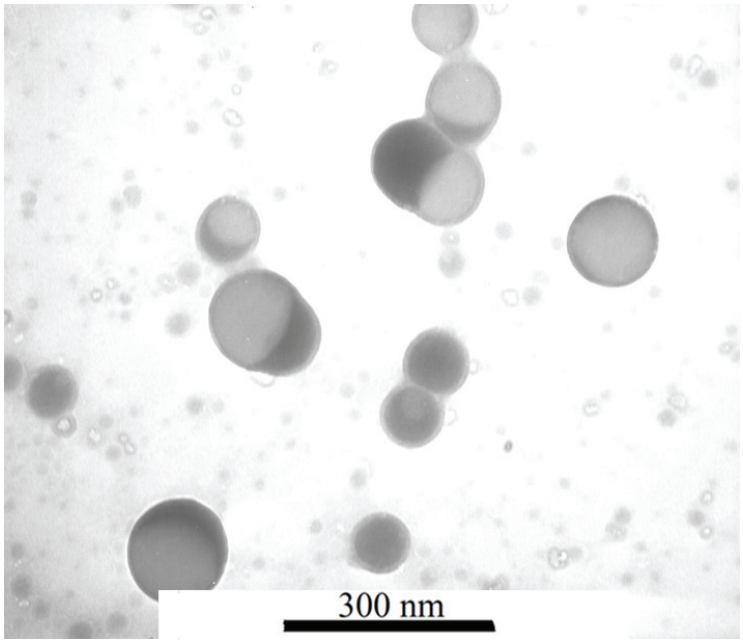

Figure 3-6 TEM micrograph of OsO_4 stained PS/PCEMA (3:1, w/w) polymer composite particles.

Figures 3-4, 3-5, and 3-6 show a mixture of occluded core-shell and acorn structures for the PS/PCEMA particles. For example, in Figure 3-4, arrow **B'** shows the acorn structure while arrow **A'** marks the occluded core-shell structure. Occluded core-shell structure is formed because of incomplete phase segregation with PS forming the core but not in the exact center of the particle, and PCEMA forming the shell. This kind of structure can be treated as a transformed core-shell structure. Aside from acorn and occluded core-shell structure particles, some particles have PCEMA shells partially surrounding PS cores (marked by arrow **C'** in Figure 3-4). We believe that this kind of morphology is the intermediate state between acorn and occluded core-shell. Figure 3-7 indicates this morphology transition.

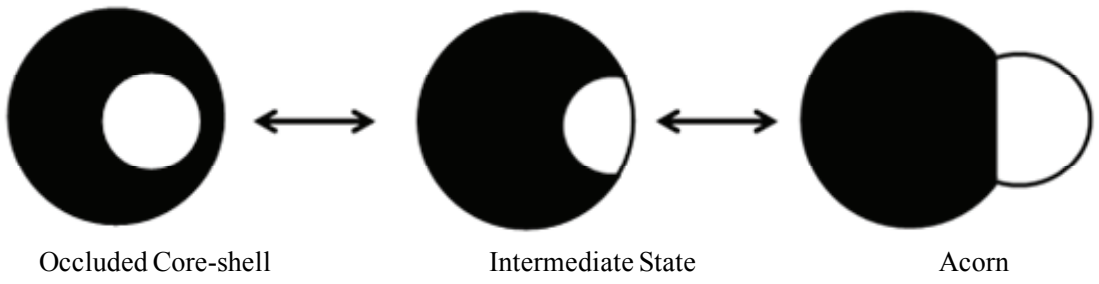

Figure 3-7 Morphology transition of PS/PCEMA composite particles

For particles containing 75%, 50%, and 25% PCEMA homopolymers by weight, the average diameters of the core consisting of both homopolymers were 48 ± 25 nm, 50 ± 21 nm, and 116 ± 44 nm, respectively. The reason that the average diameter of the particles containing 25% PCEMA by weight is larger than the other two weight ratios studied is that less surfactant was used in the preparation of particles.

Some particles show a clear phase separation in TEM images, while others appear uniformly dark or light, as marked by arrow **A** in Figure 3-1. This could be due to two reasons. For particles with a hemispherical structure, due to the different angles of projections of the particles, only when the interface between the two phases is exactly parallel with the direction of electron beam, would it show perfect "half-half" contrast. If the interface is perpendicular to the direction of the electron beam, the particle would be uniformly dark. If there is an angle between the interface and electron beam direction, the decreasing contrast would make the particle show hemisphere structure with one of the components being the major part, as marked by arrow **C** in Figure 3-2. Figure 3-8 illustrates these three cases and the corresponding TEM images.

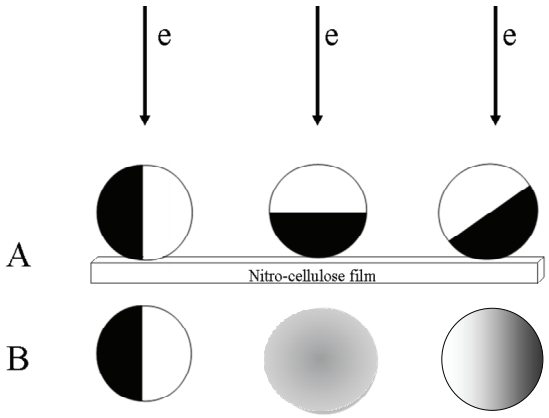

Figure 3-8 Projections from different angles for particles with hemispherical morphology. (A) Orientations of particles and electron beam direction (B) Corresponding images shown with TEM.

The second explanation for this observation is incomplete phase segregation due to the confined volume and viscosity. For example, in the PAEMA domains of these particles, there are inevitably some PCEMA chains, and vice versa. This incomplete phase

segregation decreased the contrast of the TEM images and altered the appearances of the particles.

The probability of the incomplete phase separation was further confirmed by the preparation of composite particles from chloroform evaporation instead of using toluene, as it has a lower boiling point than toluene. The emulsion was mechanically stirred at 45^{o}C for 1 hour, and then the temperature was raised to 65^{o}C to evaporate the chloroform. TEM images show that the phase separation between homopolymers was not clear and only after annealing overnight at 85 ^{o}C did their phase separation improve. Chloroform at 45^{o}C is near its boiling point but below the glass transition temperature (T_g) of PCEMA (T_g of PCEMA is about 68 ^{o}C). The existing of chloroform allows the homopolymer chains to be mobile. During chloroform evaporation, the viscosity increases, correspondingly, decreasing the mobility of the chains. At 65 ^{o}C, which is higher than the boiling point of chloroform but still lower than T_g of PCEMA, the homopolymers are in the glassy state and cannot move anymore. Only when the temperature is above the T_g, such as 85 ^{o}C or higher, would chains be mobile, allowing for phase separation. Figure 3-9 (A) shows the TEM image of PAEMA/PCEMA particles made from chloroform evaporation and Figure 3-9 (B) shows the same sample after annealing at 85^{o}C overnight.

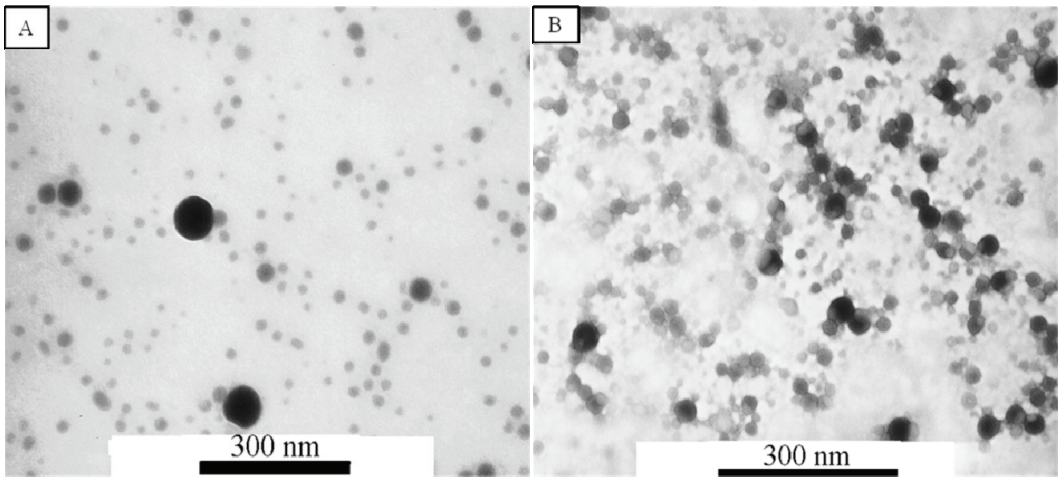

Figure 3-9 TEM micrograph of PAEMA/PCEMA (1:1, w/w) polymer composite particles after chloroform evaporation, (A) without annealing; (B) after annealing at 85^0C overnight

In order to study the influence of homopolymer weight ratio on morphology, a series of particles with different PCEMA weight ratios were made for both systems. After analyzing the TEM images, it was found that the preferred morphologies for both PAEMA/PCEMA and PS/PCEMA particles do not change for the weight ratios investigated. Furthermore, it was found that the weight ratio in each particle is not the same as the overall weight ratio. This suggests that the polymer in a single sphere is not uniformly distributed. For example, in the PAEMA/PCEMA (3:1, w/w) composite particles, perfect hemispherical particles were found where each component accounted for 50 percent of the volume of the particle, such as the particle marked by arrow **B** in Figure 3-1. This random distribution could be due to four reasons. The first reason is the different angles of projections of the particles, which have already been explained (Figure 3-8). The second reason is incomplete phase segregation. Each homopolymer domain

contains some chains of the second kind of polymer. This incomplete phase segregation decreased the contrast of TEM images, making it difficult to determine the exact weight ratio. The third reason for this observation may be due to the photo-cross-linkable property of PCEMA. After being irradiated by UV light, PCEMA domains can be crosslinked. During the synthesis of homopolymers and preparation of composite particles, it is possible that light shined on the PCEMA blocks. Thus, the PCEMA chains could crosslink with each other and form network structures. This could decrease the amount of the unsaturated carbon-carbon bonds at the same time, which consequently further decreased the contrast of TEM images. The fourth reason is that the weight ratio of homopolymers in the individual oil droplets were distributed irregularly, probably in a Poisson distribution, and consequently, particles have non-uniform weight ratios.

3.4 Atomic Force Microscopy

AFM was used in this work to analyze the topography of the composite polymer particles. The topographic images for composite particles of different weight ratios were similar, and therefore only the images for particles with a 1:1 weight ratio are presented. Figure 3-10 and Figure 3-11 show the PAEMA/PCEMA and PS/PCEMA composite particles respectively. The average diameters of these particles were measured from AFM images where the PAEMA/PCEMA (1:1, w/w) particles had an average diameter, d_{AFM}, of 92±16 nm and the PS/PCEMA (1:1, w/w) particles had an average diameter, d_{AFM}, of 66±18 nm.

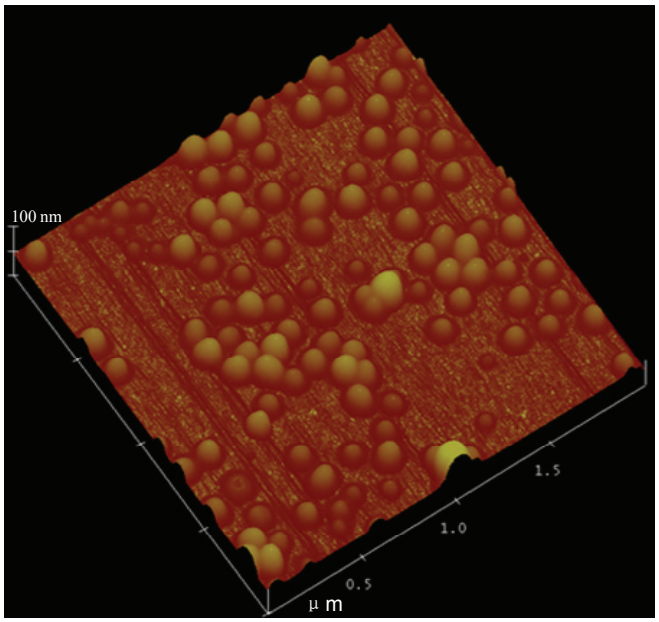

Figure 3-10 AFM topography image of PAEMA/PCEMA (1:1, w/w) polymer composite particles

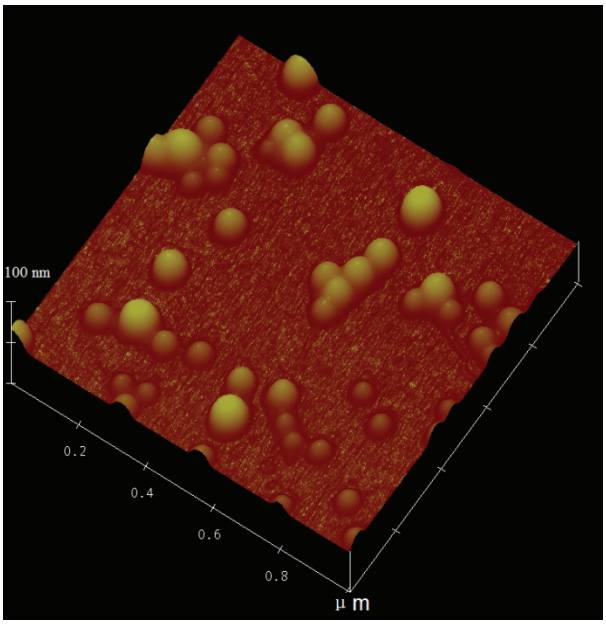

Figure 3-11 AFM image of PS/PCEMA (1:1, w/w) polymer composite particles

A disadvantage of the AFM images is that they cannot give clear and detailed information about the phase separation for the PAEMA/PCEMA and PS/PCEMA particles as the thickness of the shell formed by the surfactants shields the inner morphology from being detected by the AFM tip. This disadvantage is further compounded when attempting to analyze the occluded core-shell structure of PS/PCEMA particles, since the TEM reveals that these particles have two layers of shells, one formed by surfactants and the other by the PCEMA homopolymers.

However, AFM topographical images still provide useful information, such as verification that these particles are spherical. Furthermore, the average diameters ± standard deviation for the PAEMA/PCEMA and PS/PCEMA particles are 92±16 nm and 66±18 nm respectively. These values are larger than the d_{TEM} (which are 46±12 nm and 50±21 nm respectively). This is reasonable as TEM gives the diameter of the homopolymers core while d_{AFM} offers a measure of the overall size of the particles including the surfactant shell and corona.

3.5 Dynamic Light Scattering

DLS was employed to analyze the polydispersity and hydrodynamic diameters of the PAEMA/PCEMA and PS/PCEMA composite particles to complement the morphological and topographical information obtained from TEM and AFM studies.

We determined the hydrodynamic diameters D_h from DLS for these two systems. For PAEMA/PCEMA (1:1, w/w) composite particles, the average D_h value is 123±1nm and for PS/PCEMA (1:1, w/w) composite particles, this value is 160±2 nm, where the numbers after "±" sign denote standard deviation. These values are larger than the d_{AFM} and d_{TEM} because AFM and TEM probed the size of the particles in their dry state while DLS probed the size of the particles in their solvated state. In an aqueous environment, the corona shells of these particles swell, increasing their diameters.

The average polydispersities of these particles were also determined from DLS analyses. The polydispersity index is the parameter to evaluate the size distribution of the particles. For PAEMA/PCEMA (1:1, w/w) composite particles, the average polydispersity is 0.30 ± 0.01; for PS/PCEMA (1:1, w/w) composite particles, the average polydispersity is 0.18 ± 0.02. These polydispersity data show that both PAEMA/PCEMA and PS/PCEMA composite particles are polydisperse system. Table 3-2 lists the data of d_{TEM}, d_{AFM}, and D_h as well as DLS polydispersities for PAEMA/PCEMA (1:1, w/w) and PS/PCEMA (1:1, w/w) composite particles.

Table 3-2 Characteristics of PAEMA/PCEMA (1:1, w/w) and PS/PCEMA (1:1, w/w) composite particles[a]

	D_h (nm)	K_2^2/K_4	d_{TEM} (nm)	d_{AFM} (nm)
PAEMA/PCEMA (1:1, w/w)	123±1	0.30±0.01	46±12	92±16
PS/PCEMA (1:1, w/w)	160±2	0.18±0.02	50±21	66±18

[a] Values are given as the average ± standard deviation

Table 3-2 compares the diameters of the particles measured from DLS, TEM, and AFM. It shows that for PAEMA/PCEMA and PS/PCEMA particles, while their d_{TEM} are close, the d_{AFM} of the PAEMA/PCEMA particle is larger than that of the PS/PCEMA particle. This may be due to the reason that the surfactant used for PAEMA/PCEMA particles is $PGMA_{300}$-P(CEMA-ran-AEMA)$_{37}$, while the surfactant used for PS/PCEMA particles is $PGMA_{100}$-$PCEMA_{15}$. The longer corona layer formed by the longer PGMA chains increases the diameter measured by the AFM tip. However, values of D_h indicate that the PS/PCEMA particles have a conflicting larger D_h than PAEMA/PCEMA particles. The existence of aggregates in the PS/PCEMA composite particles can explain this abnormality as the aggregates formed by composite particles would increase the D_h value. When compared with the PAEMA/PCEMA composite particles, the surfactants used in the PS/PCEMA composite particles had shorter PGMA chains and thus, the repulsions between composite particles caused by PGMA chains are less than those of the PAEMA/PCEMA composite particles. This makes it more likely that the PS/PCEMA particles will aggregate in the aqueous solution. When using AFM and TEM images to calculate the diameter, it is easier to distinguish composite particles from micelles and aggregates and the average diameters measured by AFM and TEM are therefore closer to the real value.

3.6 Theoretical Calculations

To predict the thermodynamic equilibrium morphology of latex polymer particles made from two components, the Gibbs free energy change is the more commonly used method[1]. The Gibbs free energy change for morphology development during phase separation can be defined by combining the terms of enthalpic, entropic and surface free energies together. As the droplets are large compared to the size of molecules, the enthalpic and entropic energy changes are negligible. Thus, the Gibbs free energy change (ΔG) can be expressed in terms of the total interfacial free energy change [2,3]. In Equation **3-1**, A_i is the area of the interface and γ_i is the interfacial tension at the *i*th interface. The $A_0\gamma_0$ term is the reference energy state.

$$\Delta G = \sum_i A_i\gamma_i - A_0\gamma_0 \qquad [3\text{-}1]$$

Theoretically, the preferred morphology at thermodynamic equilibrium is the one with the lowest total interfacial free energy changes. Since the organic solvents are removed from the system in the last step, the only interfacial tensions that exist are those between the two polymers and the water, and between the polymers themselves.

In this work, only four simple cases are considered: (1) core-shell, (2) inverted core-shell, (3) hemi-sphere, and (4) individual spheres. Figure 3-12 shows these four morphologies and a reference state. Since the four morphologies will have the same reference state, the energy of the reference state can be neglected for comparison purposes only.

$$G = \sum_i A_i\gamma_i \qquad [3\text{-}2]$$

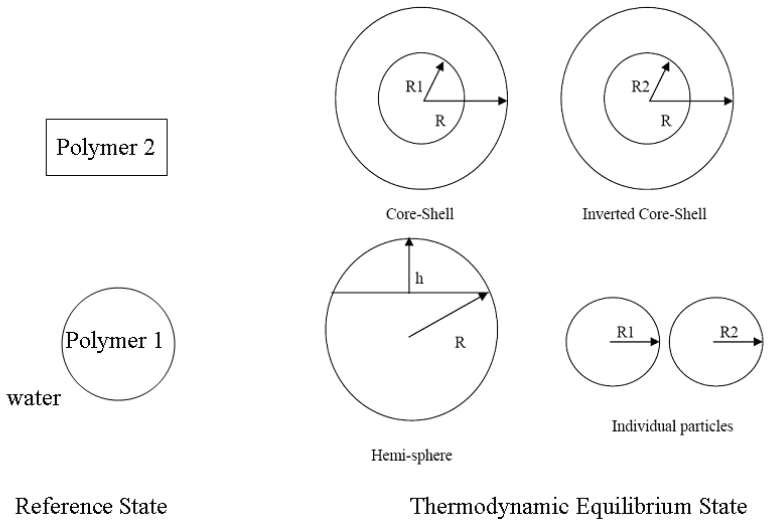

Figure 3-12 Morphology at reference state and basic morphologies at thermodynamic equilibrium state

Thus, the most preferred morphology of these four basic morphologies is the one with the lowest total interfacial free energy:

$$\begin{aligned} G_{core-shell} &= 4\pi R^2\gamma_{2w} + 4\pi R_1^2\gamma_{12} \\ G_{invertedcore-shell} &= 4\pi R^2\gamma_{1w} + 4\pi R_2^2\gamma_{12} \\ G_{hemisphere} &= 2\pi Rh\gamma_{1w} + (4\pi R^2 - 2\pi Rh)\gamma_{2w} + (2\pi Rh - \pi h^2)\gamma_{12} \\ G_{indivudual-particles} &= 4\pi R_1^2\gamma_{1w} + 4\pi R_2^2\gamma_{2w} \end{aligned} \qquad [3\text{-}3]$$

Here $\mathbf{R_1}$ and $\mathbf{R_2}$ stand for the radius of spheres formed by polymer **1** and polymer **2** respectively. **R** represents the radius of the whole composite particle, **h** the hemispherical cap thickness, and γ_{1w}, γ_{2w} and γ_{12} are the interfacial tensions between polymer **1** and water, polymer **2** and water, and polymer **1** and polymer **2** respectively. Knowing that $V_1/(V_1+V_2)=\alpha$, for the hemispherical morphology where $\alpha = 0.75(h/R)^2 - 0.25(h/R)^3$, that the surface area of the hemispherical cap is $2\pi Rh$, and that the interfacial area

between polymer **1** and polymer **2** is $2\pi Rh - \pi h^2$, equation **3-3** can be expressed in terms of the free energy per unit of polymer/water interfacial area:

$$\begin{aligned}
\gamma_{core-shell} &= \gamma_{2w} + \gamma_{12}\alpha^{2/3} \\
\gamma_{inverted-coe-shell} &= \gamma_{1w} + \gamma_{12}(1-\alpha)^{2/3} \\
\gamma_{hemisphere} &= 0.5\{\gamma_{1w}\frac{h}{R} + (2-\frac{h}{R})\gamma_{2w} + \gamma_{12}[\frac{h}{R} - 0.5(\frac{h}{R})^2]\} \\
\gamma_{indivudual-particles} &= \gamma_{1w}\alpha^{2/3} + \gamma_{2w}(1-\alpha)^{2/3}
\end{aligned} \qquad [3\text{-}4]$$

Applying the interfacial tensions between the polymer/polymer and polymer/water interfaces into equation **3-4**, the free energy per unit interfacial area for each of the morphologies can be solved.

3.6.1 Contact Angle Measurements

In order to determine the interfacial tensions between the polymer/water interfaces, the contact angle measurement method was employed. By placing a droplet of liquid on a polymer film a contact angle is formed at the solid/liquid/vapour interface where the solid surface contacts the liquid drop. At the thermodynamic equilibrium state, the relation between the contact angle and the interfacial energies is described by Young's equation which is expressed as:

$$\gamma_{SG} = \gamma_{SL} + \gamma_{LG}\cos\theta \qquad [3\text{-}5]$$

where γ_{SG}, γ_{SL} and γ_{LG} stand for solid-gas, solid-liquid and liquid-gas interfacial energies respectively, and θ is the experimental contact angle. In most literature, γ_{SG} and γ_{LG} are written as γ_S and γ_L. By knowing γ_S and γ_L, and experimentally determining the contact

angle, the interfacial energy between solid substrate and droplet can be determined. The contact angles of a water droplet on PS, PCEMA, and PAEMA polymer film substrates were measured under the same conditions with the images shown in Figure 3-13, Figure 3-14 and Figure 3-15 respectively. Five consistent measurements were done and the average value from both the left and right sides of the droplet were used to calculate as the final data value. Table 3-3 presents the average angles a water droplet assumes for each polymer substrate.

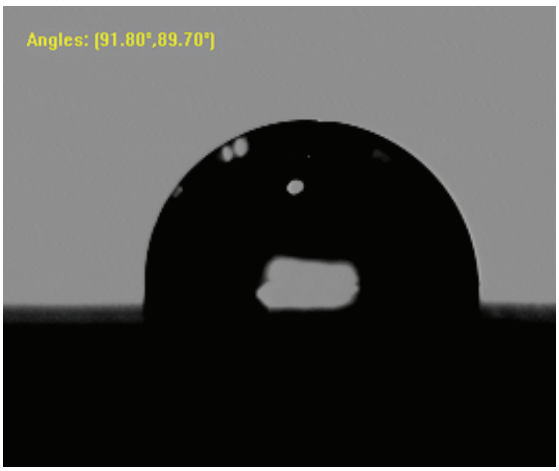

Figure 3-13 Contact angle measured for a water droplet on a PS film substrate.

Figure 3-14 Contact angle measured for a water droplet on a PAEMA film substrate.

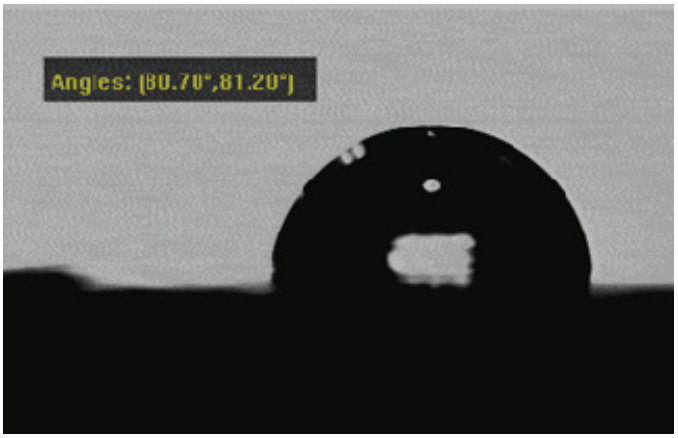

Figure 3-15 Contact angle measured of water droplet on PCEMA film substrate.

Table 3-3 Contact angles measured for water droplets on PAEMA, PS and PCEMA polymer film substrates.

	PAEMA (degrees)	PS (degrees)	PCEMA (degrees)
Water	73.3 ± 1.5	92.0 ± 1.9	80.9 ± 1.6

The data listed in Table 3-3 clearly show that among the three polymers, PS is the most hydrophobic, having the biggest contact angle with water droplet, followed by PCEMA and PAEMA in terms of hydrophobicity.

3.6.2 Surface Tension and Interfacial Tension Calculations

In order to determine the interfacial tension between the polymer and the water phases, another relation should be sought, since the surface tension of the polymer substrates used in this work could not be found from literature. Combining Young's equation with geometric mean theory, this problem can be solved. In this method, interfacial tension is defined in terms of the work of adhesion, W_a, for an equilibrium system in which a liquid with surface tension γ_L is on a solid with surface tension γ_S.

$$W_a = \gamma_S + \gamma_L - \gamma_{SL} \qquad [3\text{-}6]$$

Based on the theory that the molecular interaction between two phases in contact is proportional to the geometric mean of the surface tensions[4] , and the surface tension consists of a dispersion (non-polar) energy component, γ^d , and a polar energy component, γ^p , equation **3-7** can be presented, which is a geometric mean approximation.

$$\begin{aligned} \gamma_{SL} &= \gamma_S + \gamma_L - 2\sqrt{\gamma_S^d \gamma_L^d} - 2\sqrt{\gamma_S^p \gamma_L^p} \\ \gamma_S &= \gamma_S^d + \gamma_S^p \\ \gamma_L &= \gamma_L^d + \gamma_L^p \end{aligned} \qquad [3\text{-}7]$$

Combining equation **3-7** with the Young's equation **3-5** and equation **3-6** yields

$$W_a = \gamma_L(1+\cos\theta) = 2\sqrt{\gamma_S^d \gamma_L^d} + 2\sqrt{\gamma_S^p \gamma_S^p} \qquad [3\text{-}8]$$

Thus, by measuring at least two different liquids having known dispersion and polar energies on the same solid surface, equation **3-8** can be solved and the surface tension of the polymer substrate can be calculated by determining its polar and non-polar energies simultaneously. It is more convenient to use equation **3-9** to calculate γ_s^d and γ_s^p for use in equation **3-8** where the parameters for liquid *i* and *j* are from literature.

$$\begin{aligned}
\gamma_s^d &= \frac{[(\frac{W_a}{2})_j(\sqrt{\gamma_L^p})_i - (\frac{W_a}{2})_i(\sqrt{\gamma_L^p})_j]^2}{D^2} \\
\gamma_s^p &= \frac{[(\frac{W_a}{2})_j(\sqrt{\gamma_L^d})_i - (\frac{W_a}{2})_i(\sqrt{\gamma_L^d})_j]^2}{D^2} \\
D &= (\sqrt{\gamma_L^p})_i(\sqrt{\gamma_L^d})_j - (\sqrt{\gamma_L^d})_i(\sqrt{\gamma_L^p})_j \\
W_a &= \gamma_L(1+\cos\theta)
\end{aligned} \qquad [3\text{-}9]$$

In this work, to calculate the surface tension of the PS, PCEMA and PAEMA homopolymers, and the interfacial tension between the polymer/water interfaces, three solvents were used: water, ethylene glycol, and polyethylene glycol. The surface tension and surface tension components (γ_L^d and γ_L^p) of these solvents have been reported in literature[5] and their values are listed in Table 3-4. The method used to measure the contact angles of the ethylene glycol and polyethylene glycol droplets on the three polymer substrates were the same as the above mentioned procedures for the measurement of the water droplets, with the results shown in Table 3-5.

Table 3-4 Liquid surface tension and surface tension components

Liquids	Surface tension γ_L (dyn/cm)	γ_L^d (dyn/cm)	γ_L^p (dyn/cm)
Water	72.8	25.0	47.8
Ethylene glycol	47.4	24.9	22.5
Polyethylene glycol	45.2	30.1	15.1

Table 3-5 Contact angles measured for water, ethylene glycol and polyethylene glycol droplets on PAEMA, PS and PCEMA polymer film substrates.

	PAEMA (degrees)	PS (degrees)	PCEMA (degrees)
Water	73.3 ± 1.5	92.0 ± 1.9	80.9 ± 1.6
Ethylene glycol	48.2 ± 1.1	63.9 ± 0.8	58.3 ± 0.6
Polyethylene glycol	39.5 ± 1.1	44.9 ± 0.5	44.8 ± 2.4

Applying these values into equation **3-9,** the surface tensions of the polymers and the interfacial tensions between each polymer and its corresponding solvents can be calculated. The final surface tension of the polymer is the average value calculated from these three solvents systems. Here the detailed calculation procedures for the PCEMA surface tension and the PCEMA/water interfacial tension are given as an example. From Table 3-5 the average contact angles formed between the PCEMA/water and PCEMA/ethylene glycol interfaces are 80.9 ± 1.6^o and 58.3 ± 0.6^o respectively. After treating water as liquid ***i*** and ethylene glycol as liquid ***j***, substituting these data into equation **3-9** results in:

$$(Wa)_i = (\gamma_L)_i(1+\cos\theta_i) = 72.8\times(1+\cos 80.9) = 84.3(dyn/cm)$$

$$(Wa)_j = (\gamma_L)_j(1+\cos\theta_j) = 47.4\times(1+\cos 58.3) = 72.4(dyn/cm)$$

$$D = (\sqrt{\gamma_L^p})_i(\sqrt{\gamma_L^d})_j - (\sqrt{\gamma_L^d})_i(\sqrt{\gamma_L^p})_j = \sqrt{47.8}\times\sqrt{24.9} - \sqrt{25}\times\sqrt{22.5} = 10.8(dyn/cm)$$

$$\gamma_s^d = \frac{[(\frac{W_a}{2})_j(\sqrt{\gamma_L^p})_i - (\frac{W_a}{2})_i(\sqrt{\gamma_L^p})_j]^2}{D^2} = \frac{(\frac{72.4}{2}\times\sqrt{47.8} - \frac{84.3}{2}\times\sqrt{22.5})^2}{10.8^2} = 21.4(dyn/cm)$$

$$\gamma_s^p = \frac{[(\frac{W_a}{2})_j(\sqrt{\gamma_L^d})_i - (\frac{W_a}{2})_i(\sqrt{\gamma_L^d})_j]^2}{D^2} = \frac{(\frac{72.4}{2}\times\sqrt{25} - \frac{84.3}{2}\times\sqrt{24.9})^2}{10.8^2} = 7.5(dyn/cm)$$

$$\gamma_s = \gamma_s^d + \gamma_s^p = 21.4 + 7.5 = 28.9(dyn/cm)$$

These same procedures are repeated for water/polyethylene glycol and ethylene glycol/polyethylene glycol liquids pairs. Then, the average values are calculated and presented as the final surface tension and surface tension components for PCEMA. Results of surface tension and surface tension components for PCEMA, PS, and PAEMA are listed in Tables 3-6, 3-7, and 3-8 respectively.

Table 3-6 PCEMA surface tension and surface tension components calculated by different liquid pairs and their average value

Liquid Pair	**Surface tension γ_S (dyn/cm)**	γ_S^d **(dyn/cm)**	γ_S^p **(dyn/cm)**
Water/Ethylene glycol	28.9	21.4	7.5
Ethylene glycol/Polyethylene glycol	42.7	42.0	0.7
Water/Polyethylene glycol	35.6	31.2	4.2
Average value	35.6	31.5	4.1

Table 3-7 PS surface tension and surface tension components calculated by different liquid pairs and their average value

Liquid Pair	Surface tension γ_S (dyn/cm)	γ_S^d (dyn/cm)	γ_S^p (dyn/cm)
Water/Ethylene glycol	41.4	41.2	0.2
Ethylene glycol/Polyethylene glycol	59.3	58.6	0.7
Water/Polyethylene glycol	49.7	49.7	0.0
Average value	50.1	49.8	0.3

Table 3-8 PAEMA surface tension and surface tension components calculated by different liquid pairs and their average value

Liquid Pair	Surface tension γ_S (dyn/cm)	γ_S^d (dyn/cm)	γ_S^p (dyn/cm)
Water/Ethylene glycol	33.4	22.1	11.3
Ethylene glycol/Polyethylene glycol	37.1	30.5	6.6
Water/Polyethylene glycol	35.7	26.2	9.5
Average value	35.4	26.3	9.1

Applying the calculated surface tension of the polymers and the experimentally determined contact angle values of the water/polymer interface into Young's equation **3-5**, the interfacial tensions between the polymers and the water can be calculated. The calculation of the interfacial tension between the PCEMA/water interface is given as an example:

$$\gamma_{PCEMA/water} = \gamma_{PCEMA} - \gamma_{water}\cos\theta = 35.6 - 72.8 \times \cos 80.9 = 24.1(dyn/cm)$$

To calculate $\gamma_{PS/water}$ and $\gamma_{PAEMA/water}$, the same procedure was used and the results are listed in Table 3-9.

Table 3-9 Interfacial tension between the polymer substrate and a water droplet

Polymer substrate	Interfacial tension (dyn/cm)
PCEMA	24.1
PS	52.6
PAEMA	14.5

In order to determine the interfacial tension between different polymers, Young's equation can be used by treating one of the polymers as a solid substrate and the other as a liquid. However, it is difficult to determine the contact angle between polymers. In order to solve this problem, Wu's equation[6] is used (equation **3-10**), which avoids the need of a contact angle. It is a harmonic mean approximation for both the dispersion and polar components. However, compared to the interfacial tension between polymer and water phases, the interfacial tension between polymers is small enough that it does not significantly affect the final morphology prediction.

$$\gamma_{SL} = \gamma_S + \gamma_L - \frac{4\gamma_S^d \gamma_L^d}{\gamma_S^d + \gamma_L^d} - \frac{4\gamma_S^p \gamma_L^p}{\gamma_S^p + \gamma_L^p} \qquad [3\text{-}10]$$

PS/PCEMA is given as an example where PCEMA is treated as a liquid. Substituting the calculated surface tensions of PCEMA and PS into equation **3-10** gives:

$$\gamma_{SL} = \gamma_S + \gamma_L - \frac{4\gamma_S^d \gamma_L^d}{\gamma_S^d + \gamma_L^d} - \frac{4\gamma_S^p \gamma_L^p}{\gamma_S^p + \gamma_L^p} = 50.1 + 35.6 - \frac{4 \times 49.8 \times 31.5}{49.8 + 31.5} - \frac{4 \times 0.3 \times 4.1}{0.3 + 4.1} = 7.4(dyn/cm)$$

$$\gamma_{PCEMA/PS} = 7.4(dyn/cm)$$

Using the same procedure to calculate the interfacial tension between PAEMA and PCEMA results in $\gamma_{PAEMA/PCEMA} = 2.4(dyn/cm)$.

3.2.1 Calculations of Free Energies for Different Morphologies

From the calculations above, the data of interfacial tensions between the polymer/water and polymer/polymer phases can be inserted into equation **3-4** to determine the free energies per unit area for the basic morphologies at thermodynamic equilibrium.

The core-shell structure of the PCEMA/PS system (1:1, w/w) is presented as an example. Assume PCEMA as polymer **1,** forming the core and PS as polymer **2,** which forms the shell. The density of PCEMA[7] and PS[8] are 1.25 g/cm^3 and 1.05 g/cm^3 respectively.

$$\gamma_{core-shell} = \gamma_{2w} + \gamma_{12}\alpha^{2/3} = \gamma_{2w} + \gamma_{12}\left(\frac{\rho_2}{\rho_1+\rho_2}\right)^{2/3} = 52.6 + 7.4 \times \left(\frac{1.05}{1.25+1.05}\right)^{2/3} = 57.0(dyn/cm)$$

The same procedure was used to calculate the free energies per unit area for the morphologies of the PS/PCEMA and PAEMA/PCEMA systems with different homopolymers weight ratios. Table 3-10 and Table 3-11 show the calculation results of the PS/PCEMA system and the PAEMA/PCEMA system respectively. In these calculations, PCEMA was always defined as polymer **1**.

Table 3-10 Free energy per unit interfacial area of PS/PCEMA system with different homopolymers weight ratios

Morphology	Core-shell (dyn/cm)	Inverted core-shell (dyn/cm)	Simple hemisphere (dyn/cm)	Individual spheres (dyn/cm)
PCEMA/PS (1:3, w/w)	55.3	30.4	45.5	53.4
PCEMA/PS (1:1, w/w)	57.0	29.0	41.0	49.3
PCEMA/PS (3:1, w/w)	58.5	27.3	35.8	42.0

Table 3-11 Free energy per unit interfacial area of PAEMA/PCEMA system with different homopolymer weight ratios

Morphology	Core-shell (dyn/cm)	Inverted core-shell (dyn/cm)	Simple hemisphere (dyn/cm)	Individual spheres (dyn/cm)
PCEMA/PAEMA (1:3, w/w)	15.5	26.1	18.2	21.6
PCEMA/PAEMA (1:1, w/w)	16.0	25.6	20.0	24.4
PCEMA/PAEMA (3:1, w/w)	16.5	25.0	21.5	25.7

Table 3-10 reveals that for the PS/PCEMA system, the morphology that has the lowest free energy per unit interfacial area is the inverted core-shell structure, with PCEMA forming the shell and PS forming the core, for all homopolymer weight ratios studied. Thus, the theoretically most preferred morphology for this system is an inverted core-shell structure. The second preferred morphology is simple hemisphere, followed by individual spheres and core-shell (PS forms the shell and PCEMA forms the core).

Similarly Table 3-11 reveals that the theoretically most preferred morphology for PAEMA/PCEMA system is core-shell, with PCEMA forming the core and PAEMA forming the shell, for all homopolymer weight ratios studied while the second preferred morphology is simple hemisphere.

3.3 Comparison of Experimental Results and Theoretical Calculations

Results of the calculations illustrate that for PS/PCEMA composite particles, the preferred morphology at a thermodynamic equilibrium state is an inverted core-shell structure with PS forming the core and PCEMA forming the shell. However, the experimental results indicate that the preferred morphology is a mixture of occluded core-shell and acorn instead of single inverted core-shell morphology. Even though occluded core-shell morphology is not a classic core-shell, as the PS core is not located in the exact center of the particles, from the viewpoint of free energy they are nearly the same. An acorn structure, whose shape is not a perfect sphere, can be approximately treated as a transformed hemispherical structure from the viewpoint of free energies. For the transitional state (PCEMA domains partially surround PS domains), its interfacial free energy could be thought to be between the values of the occluded core-shell and the acorn structures approximately. Thus, based on these analyses we can conclude that for PS/PCEMA system the theoretical calculations partially agree with the experimental results.

The analysis for the PCEMA/PAEMA system is done similarly. For this system, the morphology with the lowest γ value is the core-shell structure where PAEMA forms the shell and PCEMA forms the core. The second preferred morphology is simple hemisphere. After comparing them with TEM images, which showed that the most preferred structure was a hemisphere, it was found that for the PAEMA/PCEMA system the theoretical calculations do not agree with the experimental results.

The disagreement between experimental results and theoretical calculations could be due to three reasons. First, the closeness of the free energies makes mixture morphologies possible. For the preferred morphology, the free energy per unit area, or γ value, is more reasonably to be a range instead of a sharp point. If two morphologies have similar γ values, they can mutually exist. Second, the uncertainty in our interfacial tension measurement could also influence the accuracy of the final free energy calculations, especially for PAEMA/PCEMA system. For the PAEMA/PCEMA system, the differences in γ between different morphologies are much smaller than those found in the PS/PCEMA system. Thus, the uncertainty during the interfacial tension calculation plays a more significant role. The third possibility for the disagreement is the high viscosity inside the particles. As toluene evaporated during particle synthesis, the viscosity increased and the chain mobility decreased, which prohibited complete phase separation. When all the organic solvents were evaporated and the emulsion was cooled down to room temperature, far below glass transition temperature (T*g*) of both PCEMA

and PS homopolymers, polymer chains were immobilized. Thus, some dynamically controlled structures could have been locked in. TEM images of PAEMA/PCEMA composite particles made from chloroform evaporation confirm the role of a kinetic influence on the final morphology, as when compared with toluene, chloroform is more easily evaporated. In the experiment, the temperature of the emulsion was kept at 45 ^{o}C for 1 hour and then rose to 65 ^{o}C to evaporate chloroform. At temperature lower than the T*g* of PCEMA, and inside the highly viscous particles, it was too difficult for the polymer chains to move. Most of the chains were frozen and phase separation was not clear. At 85 ^{o}C, which was above the T*g* of PCEMA, the mobility of the polymer chains increased and the incompatible chains preferred to form their own domains. Thus after 1 day high temperature annealing, the phase separation became more clear.

3.4 Conclusions

In this chapter, the morphology and topography of PAEMA/PCEMA and PS/PCEMA composite particles were studied using TEM, AFM, and DLS. The results indicate that these particles are polydisperse and nano-size spheres. For PAEMA/PCEMA particles, the preferred morphology is hemispherical, while for PS/PCEMA particles the morphology is a mixture of acorn and occluded core-shell. Furthermore, based on the Gibbs free energy change theory, predictions of morphologies at the thermodynamic state were made and though these calculations only partially agreed with the experimental

observations, they allow for the preparation of composite polymer particles with the desired morphologies by taking these predictions into account.

Acknowledgement

I am grateful to Jian Wang for her help with the AFM work, Yang Gao for helping with theoretical calculation and contact angle measurement work.

References

1. Sundberg, D.C.; Durant, Y.G.; *Polym.React. Eng.* **2003**, *11*, 379
2. Berg, J.; Sundberg, D.C.; Kronerg, B.J.; *Microencap.* **1989,** *6666*, 327
3. Sundberg, D.C.; Casassa, A. P.; Pantazopoulos, J.; Muscato, M. R. *J.Appl. Polym. Sci.* **1990**, 41, 1425
4. Fowkes, F.M.; "Chemistry and Physics of Interfaces", Am. Chem. Soc., Washington, D.C., **1965**
5. Saito, M; Yabe, A.; *Tex. Res. J.* **1983**, *53*, 54
6. Wu, S.; *J. Colloid Interface Sci.* **1969,** *31***,** 153
7. Liu, G.J.; Ding, J.F.; Hashimoto, T.; Kimishima, K.; Winnik, M.; Nigam, S.; *Chem. Mater.* **1999,** *11,* 2233
8. Mark, James E., *Physical properties of polymers handbook(2nd ed.)*, New York: Springer, 2007

Chapter 4
Summary and Conclusions

4.1 Formation of Composite Polymer nano-Particles

I have prepared PAEMA/PCEMA and PS/PCEMA composite nano-particles using the oil in water emulsion method. In this work, the artificial route was chosen. With the aid of simple mechanical stirring, nano-particles can be formed. From the preparation of PAEMA/PCEMA and PS/PCEMA composite particles, particles with hemisphere structures and a mixture of core-shell and acorn structures, respectively were obtained.

In this work, TEM, AFM, and DLS were employed to study the morphology and topology of the PAEMA/PCEMA and PS/PCEMA composite particles. With the help of target staining, the position of each homopolymer was pointed out, and thus the morphologies were studied. In addition, by using AFM, the topology of the particles was studied. Results indicate that they are spherical particles. DLS analysis shows that these kinds of particles are polydisperse.

4.2 Theoretical Calculations

Thermodynamic equilibrium method was used in this study to predict the equilibrium morphologies of the PAEMA/PCEMA and PS/PCEMA composite particles. Due to the fact that the droplets were large compared to the size of molecules, the enthalpic and entropic energy changes were negligible. To obtain the interfacial tensions between

homopolymers, Wu's equation was used as an approximation method. To obtain the surface tension of polymers and interfacial tensions between polymers and water droplet, Saito's and Young's equations were used. All of the above calculations were based on the data provided by the contact angle measurements. Due to the uncertainties resulting from the contact angle measurements and approximations during calculations, the final theoretical calculations only partially agree with the experimental observations.

4.3 Significance of Work

It is known that composite polymer particles have broad applications with better properties and functions compared with single component materials. In this study, PS/PCEMA and PAEMA/PCEMA composite particles were prepared with $PGMA_{100}$-$PCEMA_{15}$ and $PGMA_{300}$-$P(CEMA\text{-}ran\text{-}AEMA)_{37}$ surfactants, respectively. Their morphologies were studied by using TEM, AFM, and DLS. By using PCEMA as homopolymers and one block of the surfactants, the structures can be locked. By using PGMA as one block of the surfactants, the particles are water dispersible so that they can be further modified and applied in the field of biology. Additionally, by further modifying the surface of the particles or changing the un-crosslinkable parts of the particles, these kinds of particles with desired morphologies could have more potential applications. In this work, based on the Gibbs free energy change theory, predictions of morphologies at the thermodynamic state were made and, though these calculations only partially agreed with the experimental observations, by taking these predictions into

account, the composite particles with desired morphologies can be prepared under some guidance.

4.4 Future Work

In this study, both kinds of composite polymer particles are polydisperse. In order to make monodisperse composite particles further studies are required. Other techniques, such as the membrane emulsification method, might prove effective. With this method, high monodisperse particles may be made.

To make the theoretical calculations closer to the experimental observations, more accurate methods of determining the interfacial tensions between polymers and polymer against water should be found. Since the presence of surfactants decreases the interfacial tensions between polymers against water, the interfacial tension between two homopolymers would play a more significant role in determining the final morphologies, Wu's equation is thus not sufficient. In order to make more accurate predictions, a more accurate method should be found.

Furthermore, based on the route of PS/PCEMA and PAEMA/PCEMA composite particles preparations, we could prepare many other kinds of composite particles by using different homopolymers or even block copolymers with desired properties and functions. For example, by using the conductive polymers, we could make composite particles with

electro-response. When other bio-compatible polymers are used, the composite particles with bio-applications could be prepared. In addition to the above, by modifying the surface of the particles, many unique compositions could be introduced, such as amines or carboxylic acids. These kinds of reactive sites make it possible to use the particles in the biology field.

Additionally, based on the spherical particles we have already made, non-spherical particles could also be prepared by merely extracting the un-crosslinkable parts from the particles. The non-spherical particles could reveal more novel responses to external fields due to their lack of spherical symmetry and have already been studied by many groups within the last 20 years.[1-3]

Reference

1. Cho, I.; Lee, K.-W. *J. Appl. Polym. Sci.* **1985**, *30*, 1903.
2. Okubo, M; Ando, M.; Yamada, A.; Katsuta, Y.; Matsumoto, T. *J. Polym. Sci. Polym. Lett. Ed.* **1981**, *19*, 143.
3. Kim, J.-W.; Larsen, R. J.; Weitz, D. A. *J. Am. Chem. Soc.* **2006**, *128*, 14374.

Appendix 1
Composite Particles Prepared with Compatibilizer or non-Neutral Surfactants

A1.1 Introduction

In Chapter 3, composite particles were made from homopolymers and diblock copolymer surfactants. TEM analyses have shown that for PAEMA/PCEMA composite particles the morphology is hemisphere, and for PS/PCEMA composite particles the morphology is a mixture of occluded core-shell and acorn. Two methods are proposed to influence the morphologies of these kinds of particles. The first is surfactant selection. It is well-known that the interaction between polymer chains depends on two parameters[1]: overall degree of polymerization (*N*) and the Flory-Huggins interaction parameter (χ) which characterizes the repulsive interaction between two chains. In Chapter 3 of this work, the surfactants used were $PGMA_{100}$-*b*-$PCEMA_{15}$ and $PGMA_{300}$-*b*-$P(CEMA\text{-}ran\text{-}AEMA)_{37}$ for PS/PCEMA and PAEMA/PCEMA composite particles, respectively. If the length of the hydrophobic block of the surfactants increases or is not a random copolymer any more, the interaction between the hydrophobic block of surfactants and PCEMA homopolymers will change. Thus, surfactants have an effect on the phase separation between PS/PAEMA and PCEMA homopolymers and will influence the final morphology of the composite particles. A second proposed method for influencing the morphologies of the PS/PCEMA composite particles is by adding PS-*b*-PCEMA block

copolymers into the homopolymer blends. It is well-known that in polymer blends a block copolymer operates as a compatibilizer, which helps to bond the two phases to each other more tightly. In this appendix, the influence that these two methods have on the morphologies of PS/PCEMA and PAEMA/PCEMA particles will be discussed.

A1.2 Experimental

A1.2.1 Polymer Synthesis and Characterization

PS, PHEMA, PS-*b*-PCEMA and PSMA-PHEMA were used for these studies. The procedure to purify monomers and prepare the diblock copolymer PSMA-PHEMA and PS-PCEMA have been previously reported[3]. PCEMA, PAEMA and the corresponding surfactants were obtained by functionalizing the polymers, as described in Chapter 2 with the results confirmed by GPC and proton NMR.

A1.2.2 Preparation of PS/PCEMA and PAEMA/PCEMA Composite Particles using $PGMA_{300}$-$PCEMA_{37}$ as the Surfactant

All preparations were carried out in a 100 mL three-neck round-bottom flask immersed in an oil bath. A hemispherically shaped Teflon stirrer was mounted to one end of a mechanical stirring shaft and inserted into the flask via the middle joint of the flask. Water (10 mL) containing 5 mg of surfactant was added into the flask. While stirring at 1000 rpm 0.40 mL of toluene containing 7 mg of each of the homoplymers was added dropwise. For PS/PCEMA composite particles, PS and PCEMA homopolymer were

added, while for PAEMA/PCEMA composite particles, PAEMA and PCEMA homopolymers were added. Afterwards, the mixture was sonicated by using Branson Digital Sonifier 102C for 10 minutes to yield an emulsion. This emulsion was then heated to 80 ºC and mechanically stirred at 1000 rpm for 1 hour, after which, the temperature was raised to 90 °C to evaporate the toluene.

A1.2.3 Preparation of PS/PCEMA/PS-PCEMA Composite Particles

The method used to prepare PS/PCEMA/PS-PCEMA composite particles with $PGMA_{300}$-$PCEMA_{37}$ as surfactant is similar to the above mentioned procedures for the preparation of PS/PCEMA particles. First, 4.5 mg of each of the homopolymers and 1 mg PS-*b*-PCEMA diblock copolymers were dissolved in 0.4 ml of toluene to make a 25 mg/ml organic phase. This was then mixed with 10 ml of water containing 4 mg of surfactants ($PGMA_{300}$-$PCEMA_{37}$) under mechanical stirring to yield a cloudy mixture. The mixture was then sonicated for 10 minutes, forming an emulsion which was further mechanically stirred for 1 hour at 1000 rpm and 80 ºC. The temperature was then raised to 90 °C to evaporate toluene. The same method was used to prepare PS/PCEMA/PS-*b*-PCEMA composite particles with $PGMA_{100}$-$PCEMA_{15}$, with $PGMA_{100}$-$PCEMA_{15}$ replacing the $PGMA_{300}$-$PCEMA_{37}$ as the surfactant.

A1.2.4 Measurements and Techniques

Exclusion chromatographic analysis was carried out at 22^{o}C on a Waters 515 system equipped with two columns (Waters Styragel HT 4 and μStyragel 500 Å) and a differential refractometer (Water 2410). The eluant was THF and the calibration standards used were monodisperse PS samples. Proton nuclear magnetic resonance (H NMR) spectra were obtained on a Bruker Avance 400 MHz spectrometer with either deuterated chloroform or pyridine or DMF as the solvent. Transmission electron microscopy (TEM) measurements were carried out on a Hitachi H-7000 instrument operated at 75 kV. The specimens for TEM were prepared by aspirating the sample solutions on nitro cellulose coated copper grids and were subsequently stained with OsO4 vapor for 1 h before observations.

A1.3 Results and Discussions

A1.3.1 Polymer Characterization

Homopolymers bought from Sigma-Aldrich and the block co-polymers used as surfactants and compatibilizers were characterized by GPC and NMR with results presented in Chapter 3. The characterization of the compatibilizer is shown in Table A1-1.

Table A1-1 Characterization of PS-*b*-PCEMA

Sample	*M*n by GPC	*M*w by GPC	*M*w/*M*n by GPC	m/n by NMR
PS-*b*-PCEMA	2.6 X 10^4	3.0 X 10^4	1.19	1/1

A1.3.2 Transmission Electron Microscopy

TEM was employed to analyze the morphologies of composite particles. Due to staining of the PCEMA double bonds by OsO_4, the TEM images are appropriately contrasted with the dark areas corresponding to the PCEMA phase and the lighter areas corresponding to the second phase (PS or PAEMA) while the PGMA phase is invisible.

Figure A1-1 shows the TEM image of PS/PCEMA/PS-PCEMA (45%:45%:10%, weight ratio) composite particles with $PGMA_{100}$-$PCEMA_{15}$ surfactants obtained after toluene evaporation.

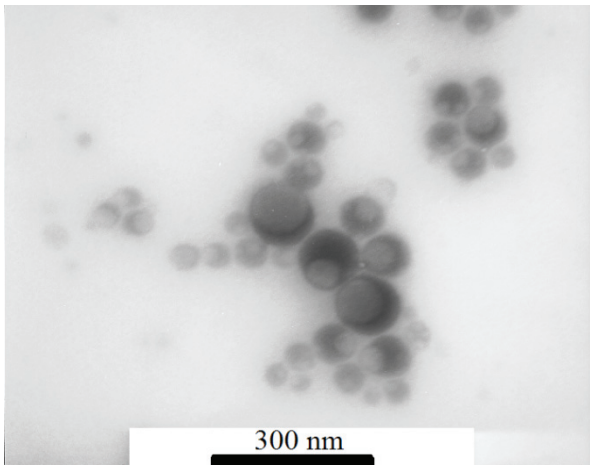

Figure A1-1 TEM micrograph of OsO_4 stained PS/PCEMA/PS-PCEMA polymer composite particles.

Figure A1-1 illustrates that the preferred morphology for PS/PCEMA/PS-PCEMA composite particles prepared using $PGMA_{100}$-*b*-$PCEMA_{15}$ as surfactants after toluene evaporation is a mixture of occluded core-shell and transition state morphologies. The PCEMA block of surfactants is supposed not to be seen since it is only 15 repeat units.

Upon adding the compatibilizer, there is nearly no acorn morphology existing. Comparing with the PS/PCEMA composite particles prepared with the same diblock copolymer surfactants, it shows that the compatibilizer made the homopolymers more miscible. The compatibilizer, PS-*b*-PCEMA block copolymer helps bond the PS and PCEMA homopolymers to each other more tightly. They lower the interfacial tension between PS and PCEMA homopolymers and make them more miscible resulting in a more homogenous mixture.

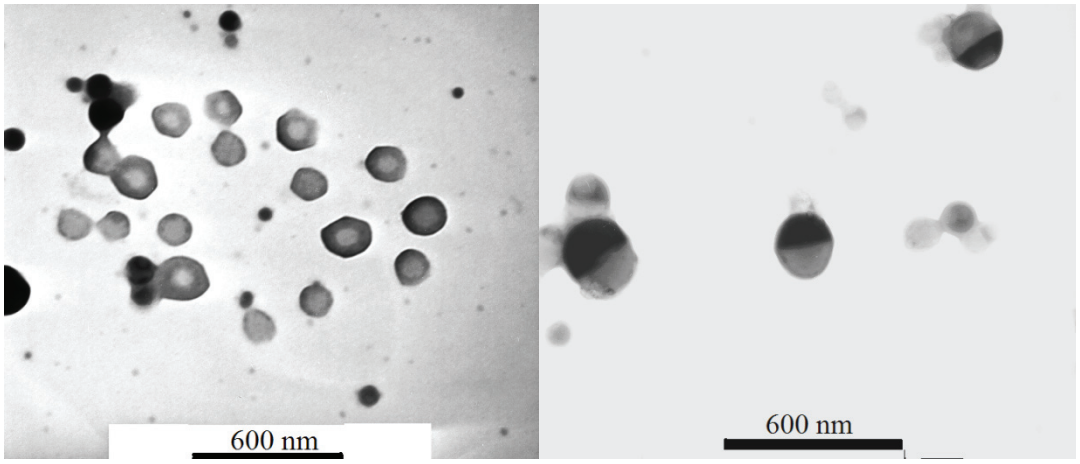

Figure A1-2 TEM micrographs of OsO_4 stained PS/PCEMA polymer composite particles prepared with $PGMA_{300}$-$PCEMA_{37}$

Figure A1-2 illustrates that the preferred morphology for PS/PCEMA (50%:50%, weight ratio) composite particles using $PGMA_{300}$-$PCEMA_{37}$ after toluene evaporation is a mixture of core-shell and hemisphere. Because the solution for TEM specimen preparation was dilute, it was difficult to get an image that contains both kinds of morphologies. In this batch, the composite particles were prepared with $PGMA_{300}$-$PCEMA_{37}$ surfactant, which has a longer hydrophobic block than $PGMA_{100}$-$PCEMA_{15}$.

As discussed before, the increasing repeat unit would increase the interaction between the hydrophobic block of surfactants and homopolymer chains. The increased degree of polymerization of the PCEMA block decreases the surfactant's miscibility with the PS homopolymers and increases its compatibility with the PCEMA homopolymers. Correspondingly, the surfactants showed more preference to PCEMA homopolymers. As a result, when comparing with the composite particles made with $PGMA_{100}$-$PCEMA_{15}$ surfactant, particles made with $PGMA_{300}$-$PCEMA_{37}$ predominantly exhibited perfect core-shell morphology. Due to the fact that the free energies of the core-shell and hemisphere morphologies are closely related, they could mutually co-exist.

Figure A1-3(A) shows the TEM image of OsO_4 stained PS/PCEMA/PS-PCEMA (46%:46%:8%, weight ratio) composite particles prepared with $PGMA_{300}$-$PCEMA_{37}$ surfactants obtained after toluene evaporation. Figure A1-3(B) presents thin section TEM image of such spheres.

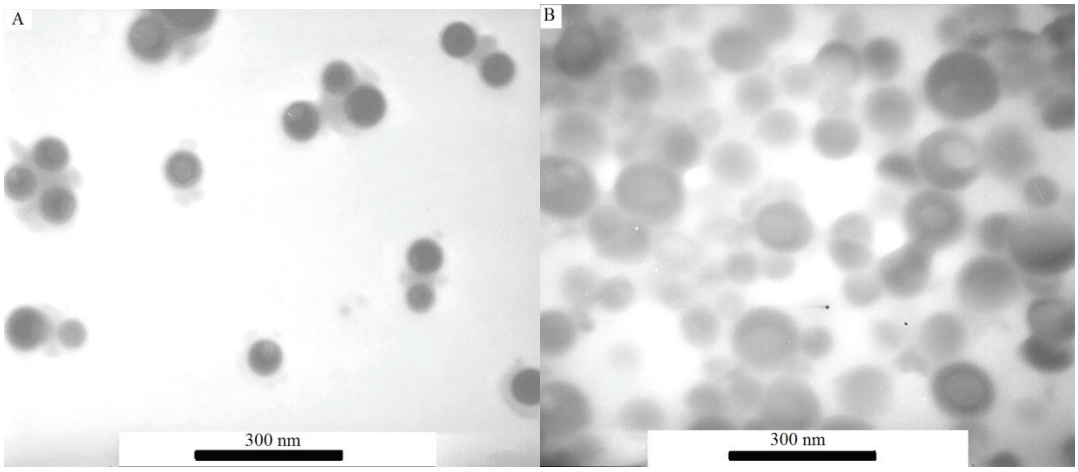

Figure A1-3 TEM micrograph of OsO_4 stained PS/PCEMA/PS-PCEMA polymer composite particles prepared with $PGMA_{300}$-$PCEMA_{37}$ (A) Spray sample, (B) Thin section of such spheres

Figure A1-3(A) and A1-3(B) illustrate that the preferred morphology for PS/PCEMA/PS-PCEMA composite particles prepared with $PGMA_{300}$-$PCEMA_{37}$ is core-shell, with PCEMA forming the shell and PS forming the core. In Figure A1-3(A), some particles show a clear phase separation, while others appear uniformly dark. This could be due to the thickness of the shells of the spheres, which is confirmed by the thin section image. In the thin section image, most of the particles clearly show a core-shell structure. These composite particles were prepared with both a compatibilizer, which decreases the incompatibility, and the $PGMA_{300}$-$PCEMA_{37}$ surfactants which show more preference to PCEMA homopolymers. Both of these factors influence the phase separation of the homopolymers.

Figure A1-4 shows a TEM image of OsO_4 stained PAEMA/PCEMA (50%:50%, weight ratio) composite particles prepared with $PGMA_{300}$-$PCEMA_{37}$ surfactants obtained after toluene evaporation and resulting in a mixture of hemisphere and triple layer structures.

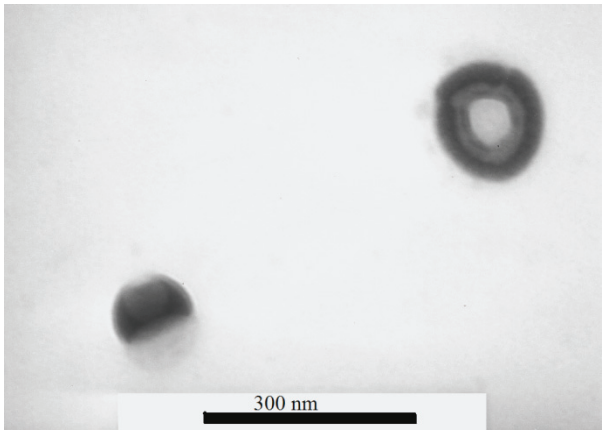

Figure A1-4 TEM micrograph of OsO_4 stained PAEMA/PCEMA polymer composite particles prepared with $PGMA_{300}$-$PCEMA_{37}$

The contrast suggests that for the triple layer morphology has an inner layer of PAEMA, an outer of PCEMA and a middle layer consisting of a mixture of the two homopolymers. When compared with the PAEMA/PCEMA composite particles prepared with $PGMA_{300}$-*b*-$P(CEMA\text{-}ran\text{-}AEMA)_{37}$ as surfactants, the particles prepared with $PGMA_{300}$-*b*-$PCEMA_{37}$ have more complex morphologies which is attributed to the surfactants' preference for the PCEMA homopolymers. As the length of the PCEMA chains in the surfactants increases, the compatibility between PAEMA and surfactants decreased. When this influence exceeds the influence of interfacial energies between homopolymers and water, the core-shell structure becomes the preferred morphology, where PAEMA

formed the core and PCEMA formed the shell. Due to the high viscosity and the confined volume, incomplete phase separation resulted in the final triple layer morphology. From the viewpoint of free energy change as the TEM image shows a mixed structure, potentially, the free energies of these two morphologies are close to one another.

A1.4 Conclusions

In this appendix, the influence of surfactants and compatibilizers on the morphology of PAEMA/PCEMA and PS/PCEMA composite particles is studied using TEM. The results indicate that both surfactants and compatibilizers affect the final morphologies of the particles. The compatibilizer helps to bond the two homopolymers together and increases their miscibility. The increased length of the hydrophobic chain in the surfactant resulted in the surfactants residing preferentially in the PCEMA homopolymer phase. This resulted in having the core-shell morphology being the preferred morphology for both PAEMA/PCEMA and PS/PCEMA composite particles. Composite particles can be formed with a specific morphology by selectively choosing the types of surfactants or through the selection of an appropriate compatibilizer.

References

1. Flory, Paul J.; *Principles of polymer chemistry*, Ithaca, Cornell University Press, 1953
2. Liu, F. T.; Liu, G. J.; *Macromolecules,* **2001,** *34,* 1302

Appendix 2

^{1}NMR Spectra

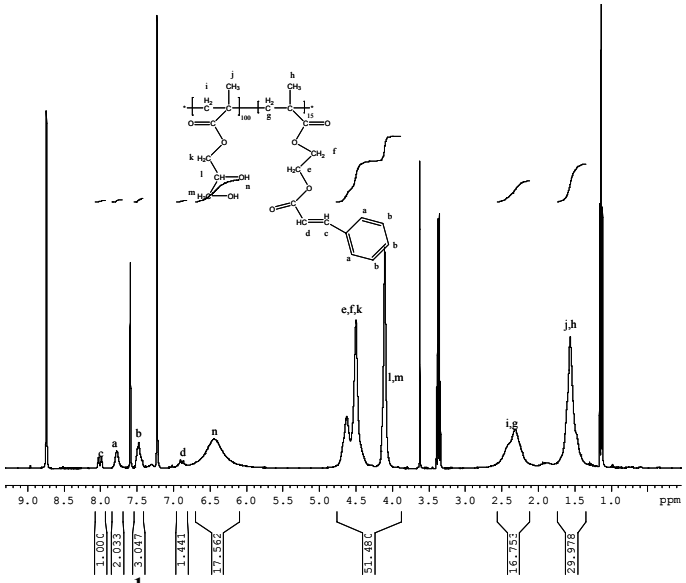

Figure A2-1: 400 MHz ^{1}H NMR spectrum of $PGMA_{100}$-$PCEMA_{15}$ in Pyridine

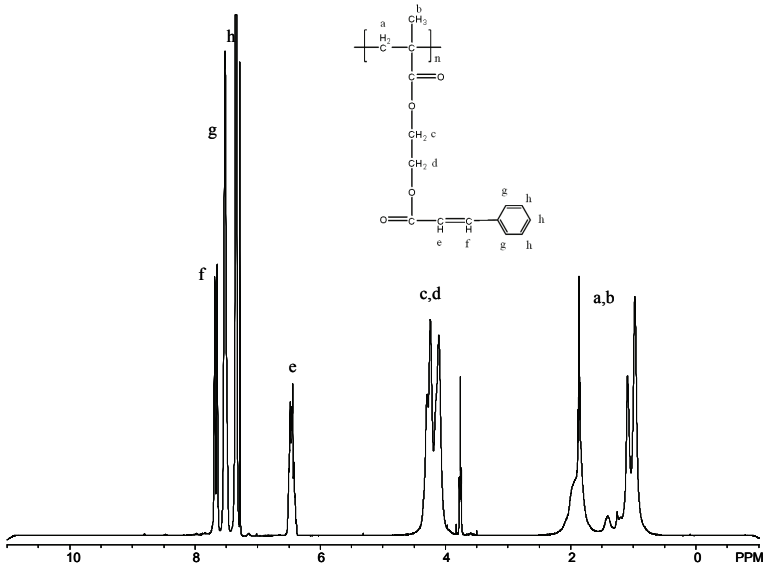

Figure A2-2: 400 MHz ^{1}H NMR spectrum of PCEMA in $CDCl_3$

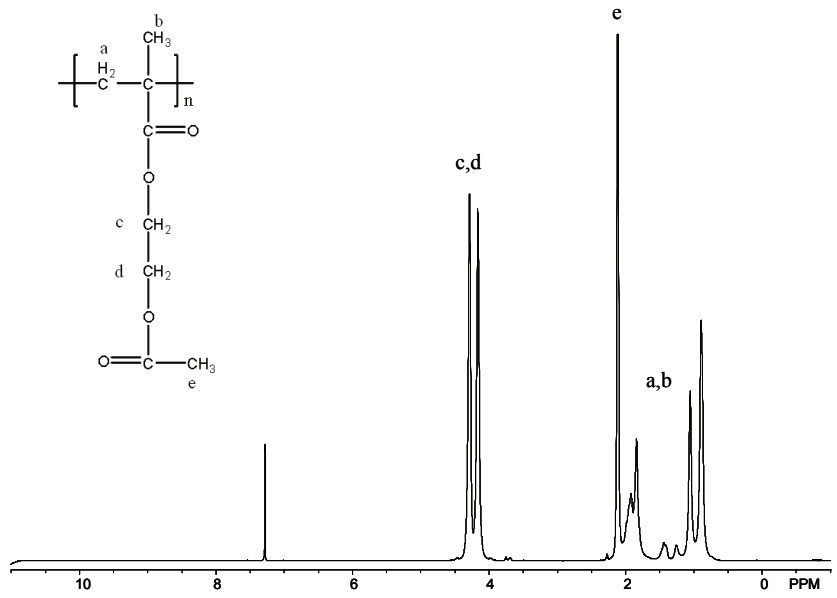

Figure A2-3: 400 MHz ^{1}H NMR spectrum of PAEMA in $CDCl_3$

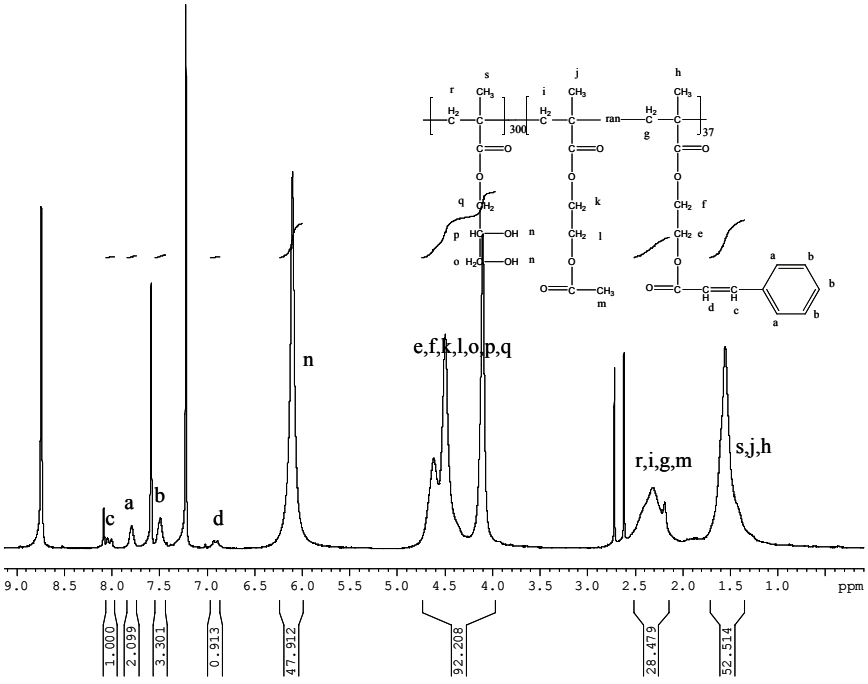

Figure A2-4: 400 MHz ^{1}H NMR spectrum of $PGMA_{300}$-P(CEMA-ran-AEMA)$_{37}$ in Pyridine

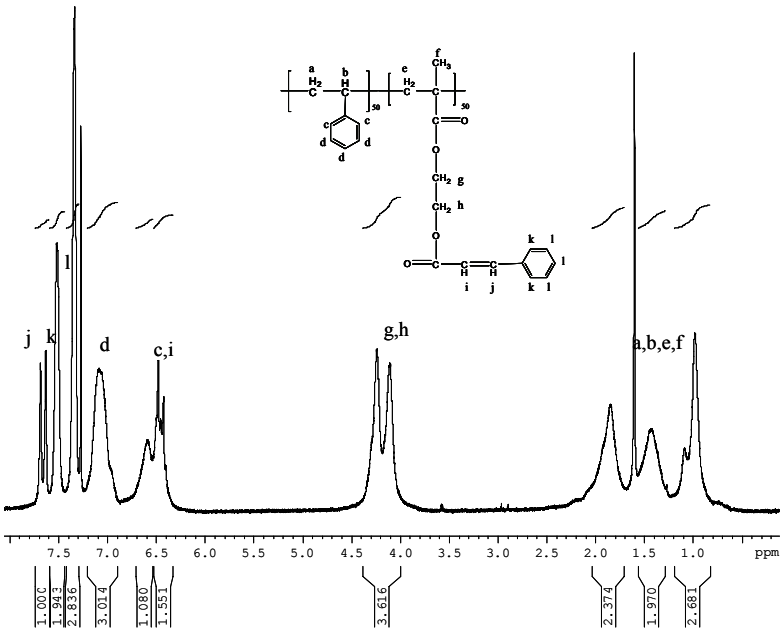

Figure A2-5: 400 MHz ^{1}H NMR spectrum of PS_{50}-$PCEMA_{50}$ in Chloroform

Appendix 3
Additional Images of Composite Particles Prepared Using SDS as Surfactants

Besides using diblock copolymer as surfactants, we also prepared PAEMA/PCEMA and PS/PCEMA composite particles by using sodium dodecyl sulfate (SDS) as surfactants. The methods used to prepare PAEMA/PCEMA/SDS and PS/PCEMA/SDS composite particles are similar to the previously mentioned procedures (in chapter 2) for the preparation of PAEMA/PCEMA/$PGMA_{300}$-*b*-P(CEMA-*ran*-$AEMA)_{37}$ particles. TEM was employed to analyze the morphologies of these composite particles. Due to staining of the PCEMA double bonds by OsO_4, the TEM images are appropriately contrasted with the dark areas corresponding to the PCEMA phase and the lighter areas corresponding to the second phase (PS or PAEMA) while the SDS phase is invisible.

Figure A3-1(A) shows the TEM image of OsO_4 stained PS/PCEMA (1:1, weight ratio) composite particles prepared with SDS surfactants obtained after toluene evaporation. Figure A1-3(B) presents thin section TEM image of such spheres.

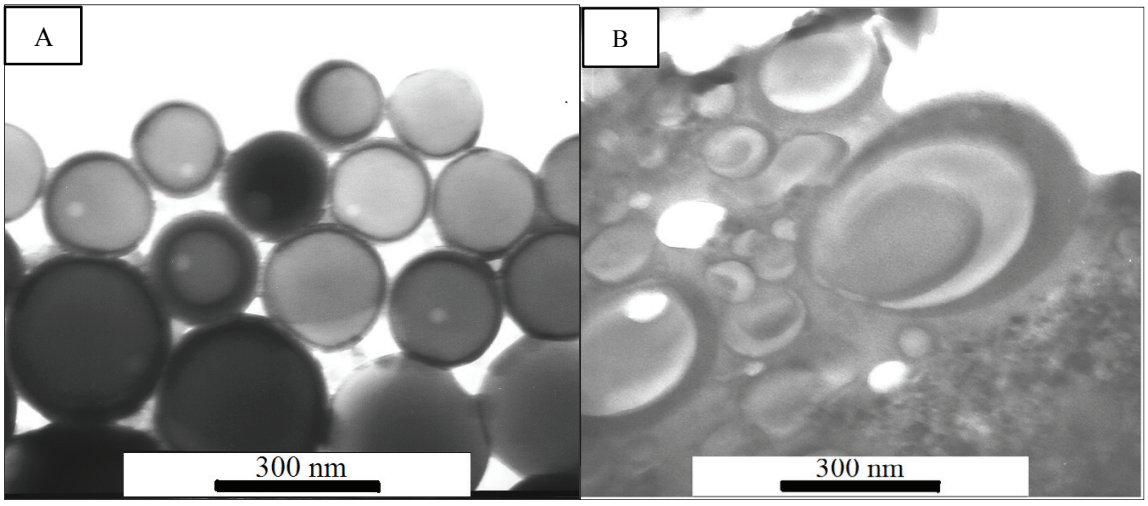

Figure A3-1: TEM micrograph of OsO_4 stained PS/PCEMA (1:1, w/w) polymer composite particles prepared with SDS (A) Spray sample, (B) Thin section of such spheres

Figure A3-2(A) shows the TEM image of OsO_4 stained PAEMA/PCEMA (1:1, weight ratio) composite particles prepared with SDS surfactants obtained after toluene evaporation. Figure A1-3(B) presents thin section TEM image of such spheres.

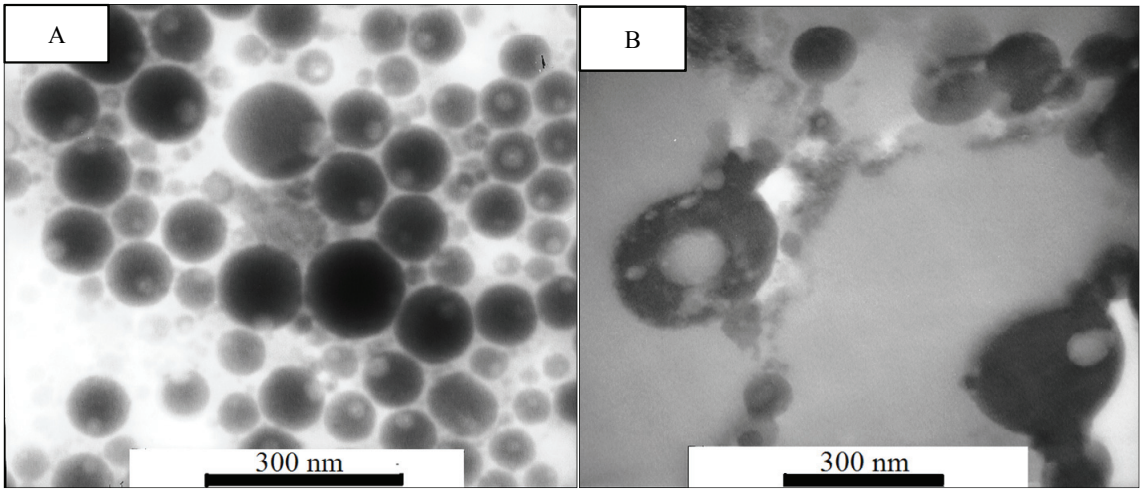

Figure A3-2: TEM micrograph of OsO_4 stained PAEMA/PCEMA (1:1, w/w) polymer composite particles prepared with SDS (A) Spray sample, (B) Thin section of such spheres